Journal of METAMORPHIC GEOLOGY

New constraints on granulite-facies metamorphism and melt production in the Lewisian Complex, northwest Scotland

Journal:	*Journal of Metamorphic Geology*
Manuscript ID	JMG-17-0090.R2
Manuscript Type:	Original Article
Date Submitted by the Author:	13-Mar-2018
Complete List of Authors:	Feisel, Yves; Johannes Gutenberg-Universitat Mainz Fachbereich Chemie Pharmazie und Geowissenschaften, Institute of Geoscience White, Richard; University of St Andrews, School of Earth and Environmental Sciences Palin, Richard; Colorado School of Mines, Department of Geology and Geological Engineering Johnson, Tim; Curtin University, Applied Geology;
Keywords:	Archaean, mafic phase equilibria, partial melting, pseudosection, THERMOCALC

New constraints on granulite-facies metamorphism and melt production in the Lewisian Complex, northwest Scotland

Yves Feisel[1], Richard W. White[1,2], Richard M. Palin[3], Tim E. Johnson[4,5]

[1] Institute of Geosciences, Johannes-Gutenberg University of Mainz, 55128 Mainz, Germany

[2] School of Earth and Environmental Sciences, The University of St Andrews, St Andrews, KY16 9AL, United Kingdom

[3] Department of Geology and Geological Engineering, Colorado School of Mines, Golden, Colorado 80401, USA

[4] Department of Applied Geology, The Institute for Geoscience Research (TIGeR), Curtin University, Perth, WA 6102, Australia

[5] State Key Lab for Geological Processes and Mineral Resources and Center for Global Tectonics, School of Earth Sciences, China University of Geosciences, Wuhan 430074, China

*Corresponding author: *yfeise02@uni-mainz.de*

Short title: Partial melting in the Lewisian Complex

ABSTRACT

In this study we investigate the metamorphic history of the Assynt and Gruinard blocks of the Archaean Lewisian Complex, northwest Scotland, which are considered by some to represent discrete crustal terranes. For samples of mafic and intermediate rocks, phase diagrams were constructed in the Na_2O–CaO–K_2O–FeO–MgO–Al_2O_3–SiO_2–H_2O–TiO_2–O_2 (NCKFMASHTO) system using whole-rock compositions. Our results indicate that all samples equilibrated at similar peak metamorphic conditions of ∼8–10 kbar and ∼900–1000 °C, consistent with field evidence for *in-situ* partial melting and the classic interpretation of the central region of the Lewisian Complex as representing a single crustal block. Melt-reintegration modelling was employed in order to estimate probable protolith compositions. Phase equilibria calculated for these modelled undepleted precursors match well with those determined for a subsolidus amphibolite from Gairloch in the southern region of the Lewisian Complex. Both subsolidus lithologies exhibit similar phase relations and potential melt fertility, with both expected to produce orthopyroxene-bearing hornblende-granulites, with or without garnet, at the conditions inferred for the Badcallian metamorphic peak. For fully hydrated protoliths, prograde melting is predicted to first occur at ∼620 °C and ∼9.5 kbar, with up to 45% partial melt predicted to form at peak conditions in a closed-system environment. Partial melts calculated for both compositions between 610 °C and 1050 °C are mostly trondhjemitic. Although the melt-reintegrated granulite is predicted to produce more potassic (granitic) melts at ∼700–900 °C, the modelled melts are consistent with the measured compositions of felsic sheets from the central region Lewisian Complex.

Keywords: Archaean; mafic phase equilibria; partial melting; pseudosection; THERMOCALC

1 INTRODUCTION

During the past c. 15 years, quantitative phase diagrams have increasingly been used to derive P–T estimates using internally consistent thermodynamic datasets containing end-members of petrological interest and activity-composition models for solid solution phases (e.g. Holland

& Powell, 1998, 2011; Johnson & White, 2011; White, Powell, & Clarke, 2003). Whole-rock specific phase diagrams—pseudosections—not only provide the opportunity to estimate P–T conditions of peak metamorphism, but may also be used to derive constraints on the prograde and retrograde path from mineral inclusions, chemical zoning, or reaction textures observed in thin section (e.g. Guevara & Caddick, 2016; Johnson & Brown, 2004; Kelsey, White, & Powell, 2003; Korhonen, Brown, Clark, & Bhattacharya, 2013; White, Powell, & Clarke, 2002).

Despite these advances, application of the pseudosection approach is limited by the availability of appropriate thermodynamic descriptions for constituent phases in the rock under study. The Earth's lower crust comprises a significant component of basic material, as evidenced by xenoliths (Rudnick & Taylor, 1987), geophysical measurements (e.g. Zandt & Ammon, 1995), and the direct examination of exhumed granulite-facies terranes (e.g. Harley, 1988; Johnson & White, 2011), which are known to have produced significant amounts of partial melt during metamorphism (Johnson, Fischer, White, Brown, & Rollinson, 2012; Sawyer, 1991). Furthermore, much of the Earth's earliest high-grade crust is typically poor in clastic sediments, with metamorphosed mafic to intermediate rocks representing valuable targets for deriving P–T conditions (e.g. White, Palin, & Green, 2017).

Until recently, activity–composition (a–x) relations for key ferromagnesian minerals commonly found within metabasic rocks, such as clinopyroxene and amphibole, were only suitable for calculating phase equilibria under subsolidus conditions (e.g. Dale, Powell, White, Elmer, & Holland, 2005; Diener & Powell, 2012; Green, Holland, & Powell, 2007). Furthermore, while effective petrological investigation of anatexis in silica-saturated siliciclastic bulk-rock compositions has been possible for over 15 years now (White, Powell, & Holland, 2001), a set of a–x relations for broadly tonalitic melt, augitic clinopyroxene, and Ti- and K-bearing amphibole, characteristic of high-grade basic and intermediate rocks, has only recently been calibrated (Green et al., 2016). These relations now allow for in-depth, quantitative investigation of granulite-facies metamorphism in the early Earth, and the formation and long-term evolution of Archaean continental crust (e.g. Johnson, Brown, Gardiner, Kirkland, & Smithies, 2017; Palin, White, & Green, 2016b; White et al., 2017).

Although the Archaean–Proterozoic Lewisian Complex of northwest Scotland is one of the most widely studied high-grade terranes on Earth, key aspects of its tectonothermal evolution remain under debate (e.g. Johnson, Fischer, & White, 2013; Johnson et al., 2012; Park, 2005; Wheeler, Park, Rollinson, & Beach, 2010, and references therein). In particular, uncertainty concerning the peak metamorphic P–T conditions for the c. 2.8–2.7 Ga granulite-facies "Badcallian" event hinders effective reconstruction of the lithospheric processes responsible for this event and limits insight into the tectonic regimes operating at this enigmatic time in Earth history. In this work, we use the a–x relations of Green et al. (2016) to model the P–T evolution of the central region of the Lewisian Complex, using calculated P–T and T–X pseudosections for 16 mafic and ultramafic rocks collected from eight localities (Figure 1). Melt reintegration modelling was carried out to reconstruct possible protolith compositions and investigate the prograde evolution and melt production during metamorphism.

Our phase equilibrium modelling shows that rocks throughout the central region of the mainland Lewisian Complex experienced near identical P–T conditions during granulite-facies metamorphism. This consistency has implications for competing tectonothermal models of the formation and is most consistent with those that involve the central region representing a singlequie coherent block.

2 REGIONAL GEOLOGY

The Lewisian Complex of north-west Scotland contains rocks with protolith ages of 3.1–2.7 Ga (e.g. Wheeler et al., 2010; Whitehouse & Kemp, 2010), which are some of the oldest rocks in Europe (e.g. Friend & Kinny, 2001; Johnson et al., 2012). These units are exposed as part of the northern foreland, a tract of rocks up to ∼20 km wide that runs from the Outer Hebrides in the north along the coast of the northwest Scottish mainland between Cape Wrath and Loch Torridon further south (Figure 1). Metamorphic rocks of the Lewisian Complex are unconformably overlain by sedimentary rocks of the Neoproterozoic Torridon group, and this entire sequence is tectonically bound to the east by the SSW–NNE trending Moine Thrust (Figure 1), and rocks of the Moine Supergroup.

The complex has been divided into the northern, central, and southern regions (Figure 1). While the northern and southern regions expose units recording mainly amphibolite-facies assemblages, the central region is primarily comprised of granulite-facies rocks (Peach et al., 1907; Sutton & Watson, 1951) considered to represent relatively deep levels of Archaean continental crust (Park & Tarney, 1987). Layered tonalite–trondjhemite–granodiorite (TTG) gneisses dominate the central region, and are intercalated with abundant sheets of metamorphosed mafic to ultramafic units, and relatively rare mica-rich supracrustal rocks (Cartwright & Barnicoat, 1987; Johnson et al., 2016; O'Hara, 1961, 1977; O'Hara & Yarwood, 1978; Park & Tarney, 1987; Zirkler, Johnson, White, & Zack, 2012). These mafic and ultramafic bodies, which include metagabbro and pyroxene-rich cumulates, may be up to several hundred metres thick and extend for many kilometres in length. All central region gneisses are cut by NW–SE trending Scourie dykes of mafic to ultramafic composition, which intruded at c. 2.4 Ga (Davies & Heaman, 2014). Historically, the Scourie dykes have been used as a relative time marker to classify metamorphic and deformation episodes either as pre-dyke (Scourian) or post-dyke (Laxfordian) (Sutton & Watson, 1951). Scourian metamorphic episodes are further divided into an earlier granulite-facies Badcallian event (c. 2.8–2.7 Ga; Corfu, Heaman, & Rogers, 1994; Zhu, O'Nions, Belshaw, & Gibb, 1997) and a later amphibolite-facies Inverian episode (c. 2.48–2.42 Ga; Evans, 1965; Zirkler et al., 2012).

Since the 1960s, a wide range of estimated P–T conditions (7–15 kbar and 700–1150 °C) for peak Badcallian metamorphism have been proposed by numerous authors (e.g. Barnicoat, 1983; Cartwright & Barnicoat, 1987; Johnson & White, 2011; Muecke, 1969; O'Hara & Yarwood, 1978; Rollinson, 1981; Sills & Rollinson, 1987; Zirkler et al., 2012). The majority of these studies focused on metamorphosed mafic and ultramafic rocks from the Scourie area for which various different conventional thermobarometers were employed. P–T estimates range from 7–9 kbar and ∼700–820 °C (Muecke, 1969; Rollinson, 1981) to 15±3 kbar and ∼1150 °C (O'Hara & Yarwood, 1978). Rare aluminous (potentially metasedimentary) rocks of the Cnoc an t'Sidhean suite yielded peak metamorphic conditions of $>$ 11 kbar and 900–1000 °C, based on thermobarometry and petrogenetic modelling in a simplified chemical system (Cartwright & Barnicoat, 1986, 1987). Phase equilibrium modelling

in the Na_2O–CaO–FeO–MgO–Al_2O_3–SiO_2–H_2O–TiO_2–O (NCFMASHTO) system was first applied to (ultra-)mafic granulites from the mainland central region of the Lewisian Complex by Johnson and White (2011). These results suggested peak metamorphic pressures of 8.5–11.5 kbar and temperatures of 875–975 °C, consistent with field evidence indicating that most metagabbroic rocks throughout the central region partially melted (Cartwright & Barnicoat, 1987; Johnson et al., 2012). Zirkler et al. (2012) employed phase equilibrium modelling of garnet-biotite gneisses ('brown' gneisses) from the Cnoc an t'Sidhean suite in the NCKFMASHTO and MnNCKFMASHTO chemical systems and proposed polymetamorphism with Badcallian peak conditions of 13–15 kbar and temperatures in excess of 900 °C. Subsequent Inverian metamorphism was characterised by the influx of H_2O-rich fluids within steep NW–SE trending shear-zones and local overprinting of Badcallian granulite-facies pyroxene-dominated assemblages to amphibolite-facies hornblende-dominated assemblages at conditions of 5–6.5 kbar and 520–550 °C. (Goodenough et al., 2010; Wheeler et al., 2010; Zirkler et al., 2012). In addition, widespread Laxfordian-aged retrogression is associated with pervasive NW–SE trending shear zones and, in places, the emplacement of pegmatitic dykes of granitic composition, especially in the northern part of the central region (Sills, 1982) along the Laxford Front (Beach, 1976).

In comparison to those in the northern and southern regions, the central-region TTG and metabasic gneisses are depleted in Si, H_2O, U, Th and some large ion lithophile elements (K, Rb, Cs) (Johnson et al., 2012; O'Hara, 1961; Rollinson, 2012; Rollinson & Windley, 1980). While several studies suggest that this depletion was the result of the partial melting and melt loss during metamorphism (Barnicoat, 1983; Cohen, O'Nions, & O'Hara, 1991; Johnson et al., 2012; Moorbath, Welke, & Gale, 1969; Rollinson, 2012) other workers favour pre-metamorphic dehydration and metasomatism of the source rocks being responsible (e.g. Rollinson & Windley, 1980; Rollinson & Tarney, 2005; Weaver & Tarney, 1981).

Opposing the classic interpretation of the Lewisian Complex as representing a single crustal block (e.g. Sutton & Watson, 1951), Friend and Kinny (2001) used geochronological data to argue that the Lewisian Complex can be subdivided in several discrete blocks or terranes, which are considered to have amalgamated during the Palaeoproterozoic (Goodenough et al., 2010; Kinny, Friend, & Love, 2005; Park, 2005). Although the idea that the

Lewisian Complex does not represent a single block of Archaean crust is becoming increasingly accepted by the community (Goodenough et al., 2010), the location of any suture zones and the corresponding timing of amalgamation are still uncertain (Wheeler et al., 2010).

3 FIELD RELATIONS AND PETROGRAPHY

A total of 72 samples were collected from eight different localities in the central region (Figure 1). Representative lithologies from each area were analysed at the Institute of Geoscience, University of Mainz, Germany, via X-ray fluorescence (XRF) for bulk-rock chemistry and electron probe microanalysis (EPMA) for individual mineral compositions. XRF analyses utilised a Philips MagiXPRO spectrometer with a rhenium X-ray tube and *in-situ* mineral analyses of one sample from each location were conducted on a JEOL JXA-8200 electron microprobe using an acceleration voltage of 15 kV, a beam current of 12 nA, and a spot size of 2 μm.

3.1 General field observations

Friend and Kinny (2001) used U-Pb geochronology to propose that the Lewisian Complex can be tectonically subdivided into discrete crustal fragments (terranes) that were subsequently amalgamated. Kinny et al. (2005) further refined this concept and proposed that the granulite-facies central region of the mainland Lewisian Complex consists of two separate allochthonous crustal fragments, namely the Assynt terrane in the north and the Gruinard terrane in the south, separated by the ∼NW–SE trending Strathan Line. While seven of the eight sample sites considered herein (Figure 1) lie within the proposed Assynt terrane, the Achiltibuie locality, found furthest south in the studied area, lies within the proposed Gruinard terrane.

The mafic bodies discussed herein that have been used for detailed thermobarometric investigation are up to tens of metres in width and hundreds of metres in length (Figure 2a). These are mostly medium- to coarse-grained metagabbro and commonly preserve relict magmatic layering. The foliations in both the TTG gneisses and metagabbroic rocks typically

dip at moderate angles. Metagabbroic layers are generally dominated by clinopyroxene, and contain varying proportions of plagioclase, hornblende, orthopyroxene, garnet, and quartz, each of which may be absent in any given locality, leading to a wide range of meso- to melanocratic, and rare leucocratic metabasic rocks. Garnet-rich metagabbro, where present, usually forms distinct layers within outcrops in which porphyroblasts of garnet are up to ∼10 cm in diameter. Orthopyroxene occurs at most localities, but may be altered to biotite and chlorite. Garnet porphyroblasts commonly exhibit prominent plagioclase-bearing coronae (Figure 2b), whose origin is consistent with high-temperature decompression (Johnson & White, 2011).

Many of the metagabbroic layers contain leucocratic quartz- and plagioclase-rich segregations (leucosomes), indicating partial melting (Johnson et al., 2013, 2012). Small-scale leucosomes, interpreted to have formed by local *in-situ* melting, occur in the melanocratic host and commonly contain large grains or accumulations of euhedral clinopyroxene (Figure 2c). In larger-scale stromatic leucosomes, pyroxene grain aggregates may also be elongated up to several centimetres in length and oriented (sub-)parallel to the foliation (Figure 2b bottom). Larger leucosomes are interpreted as having been derived *in-source*, although others feed into and are petrographically continuous with larger sheets and veins of tonalitic composition. In places large leucosomes may be separated from the host rock by pronounced mafic selvedges consistent with them representing injected melt (Figure 2d) (e.g. Diener, White, & Hudson, 2014; Johnson et al., 2013, 2012; White & Powell, 2010).

In this study, two metagabbroic rocks from each of the eight central-region localities shown on Figure 1 were used for detailed petrological analysis and modelling, comprising sixteen samples in total. This comparatively large sample set permits an assessment of the thermobarometric conditions of metamorphism across a wide spatial area of the central region of the Lewisian Complex. However, for brevity, detailed results of our modelling is only presented for six samples, which are representative of the entire set. The calculated pseudosections for the other samples are presented as supplementary information. The sample pairs from each locality were collected from the same outcrop, and where possible, were selected based on having different mineral assemblages that formed under equivalent metamorphic conditions (e.g. a garnet-bearing sample and a garnet-absent sample). Some samples show

compositional layering on a centimetre- to millimetre-scale.

3.2 Petrology and mineral chemistry of all studied samples

Most of the metabasic rocks sampled are medium- to coarse-grained, with granoblastic textures. In all localities, granulite-facies mineral assemblages are characterised by abundant clinopyroxene and plagioclase, with garnet, orthopyroxene and hornblende common in many samples. However, all of the six samples emphasised in this study contain orthopyroxene and all but two contain garnet (Table 1). Minor ilmenite, rare magnetite and accessory sulphide phases also occur.

Mineral composition analyses indicate that almost all major minerals in all studied samples lack any significant inter- or intragranular compositional variation, with the exception of matrix versus coronal plagioclase. Matrix plagioclase in most samples is subhedral, up to 1 mm in size, and relatively Ca-poor (X_{An} = 0.3–0.6 [= Ca/(Ca + Na + K)]), whereas that in coronae around garnet in samples 16AC01 and 16SC07 (Table 1) is relatively Ca-rich (X_{An} = 0.7–0.9). Pale green clinopyroxene in all studied samples is subhedral to euhedral and equigranular, with individual grains up to 1.5 mm in size, and forms coarse granoblastic aggregates. Grains in all samples are diopside/augite, with X_{Mg} = 0.6–0.8 [= Mg/(Mg + Fe)] (Table 1), with low amounts of Na (0.02–0.12 a.p.f.u.) and Al (0.02–0.29 a.p.f.u.). Garnet, where present (Table 1), occurs as large porphyroblasts up to 6 mm in diameter in the thin sections studied, though much larger grains up to 10 cm occur in the outcrops. Garnet may also be surrounded by symplectites or coronae. These reaction rims comprise an inner layer of granoblastic plagioclase, with or without minor orthopyroxene or hornblende adjacent to the porphyroblast and an outer discontinuous layer of orthopyroxene adjacent to the matrix (Figure 3a). These porphyroblasts also commonly have irregular cuspate margins, which in some cases is manifested by garnet vermicules overgrowing other minerals within the corona (e.g. 16ST02; Figure 3b). In some samples, garnet forms inclusion-rich anhedral porphyroblasts without any clear plagioclase-rich corona (e.g. 16BA04). While representative compositions of garnet varied between samples, internal compositional zoning was not recorded in any of the analysed porphyroblasts. Grains are generally Fe-rich

(X_{Alm} = 0.42–0.63 [= Fe/(Fe+Mg+Ca)]), with lesser amount of Mg (X_{Pyr} = 0.08–0.37 [= Mg/(Fe+Mg+Ca)]) and Ca (X_{Grs} = 0.04–0.26 [= Ca/(Fe+Mg+Ca)]).

Matrix orthopyroxene, where present, occurs as individual subhedral to anhedral grains, or as aggregates within the clinopyroxene–plagioclase matrix. No consistent variation in composition was observed within or between samples (X_{Mg} = 0.53–0.68). Subhedral amphibole is present in most samples disseminated throughout plagioclase–clinopyroxene matrices. Grains are generally dark-green to brown in colour, and may contain abundant fine-grained inclusions of Fe–Ti oxides, making some grains almost opaque. Samples exhibiting little to no retrogression are characterised by pargasitic amphibole, while more retrogressed samples from Tarbet (16TA07 and 16TA08) contain magnesiohornblende (cf. Hawthorne et al., 2012). Larger grains of Fe–Ti oxides commonly occur individually on triple junctions of clinopyroxene or within orthopyroxene-rich corona layers around garnet. Grains are typically ilmenite with rare exsolution lamellae of hematite or rare grains of magnetite. Large individual grains may be rimmed by a prominent fringe of garnet, containing rare symplectic intergrowths of garnet and ilmenite (Figure 3c).

Some samples (e.g. 16SC03) exhibited prominent leucosomes with either large elongated quartz grains up to 5 mm in length, or smaller interstitial quartz with very small apparent dihedral angles between surrounding plagioclase feldspar (Figure 3d). These microstructural features imply that partial melting occurred (e.g. Holness, Cesare, & Sawyer, 2011), consistent with observations from other studies in the Assynt terrane (Johnson et al., 2012).

The majority of studied samples contains small amounts of apatite and show only minor retrograde alteration, typically characterised by fine-grained chlorite or biotite forming a narrow fringe around orthopyroxene and clinopyroxene. In some places, this phyllosilicate mantle also contains fine-grained opaque material. Some samples (e.g. 16TA07, 16AS04) show more extensive retrogression, with both pyroxenes being partly or completely replaced by blueish-green amphibole, and plagioclase being strongly sericitised. Retrogression of clinopyroxene is particularly prominent along cleavage planes.

4 PHASE EQUILIBRIUM CONSTRAINTS ON THE CONDITIONS OF METAMORPHISM

All calculations were performed using THERMOCALC v3.45i (Powell & Holland, 1988) and the internally consistent dataset ds62 of Holland and Powell (2011), updated 6/2/2012. Calculations were undertaken in the NCKFMASHTO system (Na_2O–CaO–K_2O–FeO–MgO–Al_2O_3–SiO_2–H_2O–TiO_2–O_2), which offers the most realistic investigation of phase equilibria in mafic to intermediate rocks. The following a–x relations were used: metabasite melt (L), augite (aug), and hornblende (hb) (Green et al., 2016); garnet (g), orthopyroxene (opx), biotite (bi), and muscovite (mu) (White, Powell, Holland, Johnson, & Green, 2014); olivine (ol) and epidote (ep) (Holland & Powell, 2011); plagioclase (pl) and K-feldspar (ksp) (Holland & Powell, 2003); magnetite–spinel (mt, sp) (White & Powell, 2002); and ilmenite–hematite (ilm, hem) (White, Powell, Holland, & Worley, 2000). Pure phases included quartz (q), aqueous fluid (H_2O), sphene (sph), and rutile (ru). Bulk-rock compositions used for calculations were obtained by X-ray fluorescence (XRF) analysis. The CaO contents of these bulk compositions were adjusted according to the measured P_2O_5 contents to account for the presence of apatite, which was observed to be the sole P-bearing phase in all samples. The ratio of ferrous to ferric iron in each sample was determined by standard titration methods, and the measured H_2O contents were based on loss on ignition (LOI). The normalised molar bulk compositions used for phase equilibrium modelling are given in Table 2.

4.1 P–T pseudosections

All phase diagrams were constructed for conditions of 750–1050 °C and 4–16 kbar, which encompass the mid- to lower-crustal tectonothermal conditions at which the Lewisian Complex is thought to have equilibrated (e.g Johnson & White, 2011; Wheeler et al., 2010; Zirkler et al., 2012). Petrological similarities between the sixteen samples studied in this work resulted in calculated P–T pseudosections that show many common features. Thus, for brevity, only six examples from the central region are presented in Figure 4 and discussed below, which are representative of all samples investigated in this study. These comprise

16SC03 and 16SC07 from Scourie, 16BA02 and 12BA04 from Badcall Bay, and 16ST02 and 16ST03 from Strathan (Table 2). Calculated pseudosections for the remaining samples are given as supplementary material.

On each pseudosection, the solidus is indicated by a thick black line and thin, dashed contours represent calculated modal proportions of melt. The limits of garnet-bearing, orthopyroxene-bearing, and hornblende-bearing assemblage fields are coloured by red, brown, and green lines, respectively. Augite is stable throughout the entire range of P–T space considered in each diagram, and plagioclase is ubiquitous in most cases, except at high-pressure–low-temperature conditions. The low-pressure limit of garnet stability typically has a weak positive $\mathrm{d}P/\mathrm{d}T$ and ranges from 5 to 7.5 kbar at 750 °C to 8 to 11 kbar at 1050 °C. Garnet-absent assemblages are commonly dominated by augite, plagioclase, orthopyroxene and hornblende at subsolidus conditions, with hornblende persisting to relatively high temperatures in some samples (>1000 °C; e.g. 16ST02, Figure 4e).

With the exception of sample 16SC03, the calculated high-pressure stability limit of orthopyroxene occurs at ∼0.5–4 kbar above the lower-pressure boundary of garnet-bearing assemblage fields, and so defines a garnet-plus-orthopyroxene assemblage field of variable width. This topological feature provides a tight constraint on the pressures of equilibration in each locality, as many pairs of samples were selected owing to them being either garnet-bearing/orthopyroxene-absent, garnet- and orthopyroxene-bearing, or orthopyroxene-bearing/garnet-absent (Table 1). Quartz is calculated to be stable at subsolidus conditions in all lithologies, but is predicted to be fully consumed with increasing temperature, particularly at low pressures, consistent with previous calculations performed on mafic bulk compositions (Palin et al., 2016). The ilmenite–rutile transition is pressure-dependent and typically occurs at 10–14 kbar (Figure 4), which also constrains metamorphic pressures of equilibration, as no rutile was observed in any of the studied samples, although this transition is more sensitive to bulk-rock oxidation state than the garnet–orthopyroxene transition. Calculated contours for modal proportions of melt are relatively steep, with a generally positive $\mathrm{d}P/\mathrm{d}T$. Melt production is generally greatest in quartz-present, hornblende–orthopyroxene-bearing assemblages, with closely spaced contours (Figure 4a,c,d) suggesting that 10–15 mol.% may be produced within ∼50 °C above the solidus.

Scourie samples 16SC03 and 16SC07 both contain clinopyroxene, orthopyroxene, plagioclase, and ilmenite, with the absence of garnet and presence of quartz in the former allowing demarcation of the upper and lower pressure limits of equilibration, respectively. Interpreted peak P–T conditions for this locality are 9–10 kbar and 970–1010 °C (Figure 5a). Badcall Bay samples 16BA02 and 16BA04, comprise the same granulite-facies assemblage, except that 16BA04 additionally contains garnet (Tab. 1). Pressure estimates can be derived from the garnet stability boundaries in each pseudosection, giving a very narrow pressure range of ∼8–9.2 kbar. The intersection of the garnet-in lines from both diagrams defines an upper temperature boundary of 990 °C while the lower temperature limit is given by the solidus in the pseudosection calculated for sample 16BA04 at ∼875 °C (Figure 5b). Strathan samples 16ST02 and 16ST03 both comprise garnet-bearing granulite-facies assemblages dominated by clinopyroxene and plagioclase, with 16ST02 additionally containing small proportions of hornblende (Tab. 1). Pressure constraints are given by the low-pressure stability of garnet and the upper boundary of hornblende, also defining the upper temperature limit at their intersection. The lower temperature boundary is defined by the solidus. The combined peak assemblage fields of both pseudosections yield metamorphic conditions of ∼920–1020 °C and 9.2–10.5 kbar (Figure 5c).

The interpreted peak metamorphic assemblages in all six samples overlap at P–T conditions of ∼8–10 kbar and ∼900–1000 °C (Figure 5d), which can be interpreted as representing peak granulite-facies metamorphism. As each pair of samples from each locality was collected in close proximity to one another, they can be interpreted as having experienced the same tectonothermal history, and thus the peak assemblage fields determined for each can be used together to give tighter constraints on the absolute P–T conditions of equilibration. Minor phases such as rutile, quartz, or magnetite were not considered for determination of P–T conditions, as they can be difficult to identify when present in very small proportions and their modelled stability may be sensitive to uncertainties in bulk rock composition and a–x models (e.g. Palin, Weller, Waters, & Dyck, 2016c).

4.2 Modelling of melt production

Widespread petrological evidence for melt production combined with the preservation of granulite-facies assemblages in the Lewisian Complex implies that the preserved rocks are residual (White & Powell, 2002). In order to understand the prograde evolution, a protolith composition is therefore required. Possible protolith compositions for the studied samples were determined by re-integrating melt assumed to have been lost during prograde metamorphism, and was achieved using the rbi-script of THERMOCALC following the method of White, Powell, and Halpin (2004). Melt reintegration was carried out for three samples along simplified isobaric P–T paths at 9.5 kbar or 8.8 kbar, and starting from peak temperatures inferred from phase equilibrium modelling (Table 3). The different pressures were chosen to ensure that the starting point of melt reintegration lies within the assemblage fields interpreted to represent the granulite-facies peak assemblage of each sample and should not significantly affect the results given the uncertainty involved in the method (White et al., 2004). At each starting point the proportion of melt was increased down temperature until the low-T boundary of the respective field was given by the stability line of a mineral rather than the solidus. The new assemblage resulted across the low-T boundary was then used to integrate another batch of melt at the intersection of the new solidus and the P–T path, until again, the low-T boundary involved the loss of a mineral rather then melt. It is possible that the resulting low-T boundary is given by the occurrence of a new phase stabilising at lower temperatures instead of the solidus. In this case the position of the solidus was recalculated using the assemblage including the new phase and melt was reintegrated at the intersection of the resulting solidus-position and the P–T path. Following this procedure, step-wise reintegration of small amounts of melt (1–8 mol.%) was repeated until the solidus achieved H_2O-saturation ($\sim$1 mol.% H_2O), which resulted in total reintegrated melt proportions of 27–39 mol.%. The resulting model 'protolith' compositions are compared with the sample compositions in Table 3 to illustrate differences between the two. The process outlined above assumes that each of the rocks modelled was fluid saturated at the solidus and the resulting pseudosections thus represent conditions of maximum melt fertility. However, if any of the samples were not fully hydrated then a somewhat lower total melt production would be

expected along with a higher solidus temperature (e.g. Palin et al., 2016).

4.2.1 Melt-reintegrated granulite

A P–T pseudosection was calculated for one of the resulting melt reintegrated compositions (16ST02*) to illustrate the predicted phase relations of a plausible protolith (Figure 6a). The temperature range was extended down to 600 °C to ensure that the solidus lies within the range of the diagram. Due largely to the increased bulk H_2O content, the pseudosection has a distinctively different topology compared to the melt-depleted composition (Figure 4e). The solidus is shifted down-temperature by around 250 °C and is strongly modified in shape. At pressures below about 9.5 kbar, the solidus is H_2O-saturated and trends to higher temperatures with decreasing pressure. Above 9.5 kbar, the calculated solidus is fluid-absent and has a more irregular shape, initially trending to higher T before trending back to lower T above 15 kbar. Predicted subsolidus assemblages are dominated by clinopyroxene, hornblende and quartz ± H_2O, plagioclase, garnet, biotite, muscovite, epidote, sphene, and K-feldspar, and agree well with common amphibolite-facies metabasic assemblages (e.g. Palin et al., 2016; Pattison, 2003).

Garnet is stable down to pressures of 8.5 kbar at 860 °C, but for lower and higher temperatures stability is restricted to higher pressures. In particular, towards lower temperatures the garnet-in line trends up pressure until intersecting the solidus at around 13 kbar and 720 °C. This trend is very different from the original pseudosection where garnet follows a relatively constant positive $\mathrm{d}P/\mathrm{d}T$ over the whole temperature range (Figure 4e). Biotite and K-feldspar are stable to upper amphibolite facies conditions with K-feldspar being stable at pressures above 8 kbar and biotite stable below this. The prograde amphibolite–granulite facies transition at medium pressures is defined by the first occurrence of orthopyroxene above temperatures of ∼820 °C in the L–opx–aug–pl–hb–q assemblage field. This contrasts with orthopyroxene stability in the pseudosection of the original composition where the orthopyroxene-in line follows a nearly isobaric trend. After crossing the orthopyroxene-in line going up temperature, the assemblage becomes quartz absent within ∼50 °C. With increasing pressure and the appearance of garnet, orthopyroxene leaves the assemblage, form-

ing clinopyroxene–plagioclase–garnet–hornblende bearing rocks typical of the high-pressure granulite facies (O'Brien & Rotzler, 2003). Melt mode proportion isopleths generally have a steep positive $\mathrm{d}P/\mathrm{d}T$, which can be negative in garnet bearing fields and indicate an increase in melt production with increasing temperature as first biotite and later hornblende are progressively consumed. Assuming closed-system conditions, up to ∼45% of partial melt is predicted to be generated following the prograde path to intermediate pressure granulite-facies conditions at which hornblende is fully consumed (∼990 °C).

The relative proportions of stable phases are illustrated on a T–mode diagram, calculated for an isobaric section at 9.5 kbar, assuming closed-system (upper) and open-system (lower) conditions (Figure 6b). Phase proportions are output as molar percent by THERMOCALC but are normalised based on one cation, providing a close approximation to volume percent. For subsolidus amphibolite conditions the predicted assemblages are dominated by hornblende, plagioclase and quartz together with smaller amounts of epidote, biotite and augite. With the onset of partial melting, biotite and epidote are consumed and the proportion of hornblende increases, coinciding with the appearance of K-feldspar. Little melt is produced below ∼800 °C but with the appearance of garnet (∼840 °C) and orthopyroxene (∼890 °C) significantly more partial melt is produced to higher temperatures involving the consumption of quartz and hornblende. The closed-system high-T granulite assemblage is dominated by plagioclase, augite and melt together with orthopyroxene and ilmenite.

Under geologically more realistic open-system conditions melt loss is expected to occur after the accumulation of sufficient melt to overcome the strength of the host rock by forming interconnected melt-networks which provide pathways for partial melt to be drained from the rock. Rosenberg and Handy (2005) suggested that this transition occurs at melt fractions of $\phi \approx 0.07$ and termed it 'melt connectivity transition' (MCT). Therefore, for open-system conditions, after accumulation of 7 % of partial melt a melt loss event of 6% is assumed (Yakymchuk & Brown, 2015), leading to a subsequent fractionation of the total bulk-rock composition and, thus changing the phase equilibria. The residual rock becomes successively enriched in mafic phases, especially augite and orthopyroxene compared to the closed-system equivalent. Additionally, the relative proportions of plagioclase at high temperatures are strongly increased and hornblende is stable up to temperatures in excess of 1000 °C.

4.2.2 Lewisian amphibolite

A mafic amphibolite composition from Johnson, Park, and Winchester (1987) (Table. 3; sample "A4") was used to calculate a P–T pseudosection in order to compare it to the results obtained by melt-reintegration (Figure 6c). The rock was collected close to Gairloch in the amphibolite-facies southern region of the Lewisian Complex and did not experience granulite-facies metamorphism or anatexis (Johnson et al., 1987; Park, Tarney, & Connelly, 2001; Wheeler et al., 2010). The H_2O content was adjusted so that the solidus was just H_2O-saturated (<1 mol.% fluid) at 7 kbar.

The general topology of the pseudosection calculated for sample A4 strongly resembles that for 16ST02*; specifically in terms of the shapes and positions of the solidus, and stability fields for garnet, orthopyroxene, and hornblende. Predicted-amphibolite facies assemblages are the same as in 16ST02* but lack the minor K-feldspar predicted in that sample. As in 16ST02* the stability of biotite and epidote is restricted to lower temperatures (T <700 °C).

Garnet is stable to slightly lower pressures of 7.5 kbar at 860 °C and follows the same trend as in 16ST02* to higher and lower temperature. The prograde amphibolite–granulite facies transition in garnet-absent assemblages is represented by the narrow L–aug–opx–hb–pl–q–ilm field (∼800–870 °C, <7.5 kbar). At higher temperatures above this field, assemblages are quartz absent. At pressures above 10 kbar, the assemblages lack orthopyroxene and are mostly dominated by clinopyroxene, garnet and hornblende ± plagioclase. Plagioclase is absent in the upper left and right corners of the diagram, representing one major distinctive feature different from sample 16ST02*. Modal proportions of partial melt indicated by thin dashed isopleths have the same topology as those in 16ST02*, with a very steep positive or negative $\mathrm{d}P/\mathrm{d}T$ and an increase in melt production to higher temperatures. In particular, the field marking the amphibolite–granulite transition is characterised by a strong increase in melt mode, represented by close isopleths. As predicted for 16ST02*, the amphibolite composition also yields 40–45% of partial melt being generated on the prograde path up to the full consumption of hornblende (∼980 °C), assuming closed-system conditions.

Modal proportions of phases predicted to stabilise during isobaric metamorphism at 9.5 kbar under closed-system (upper) and open-system (lower) conditions are shown in Figure

6d. These assemblages are dominated by hornblende with small amounts of quartz and minor augite, biotite, epidote, and sphene at subsolidus conditions, and are generally similar to those shown in Figure 6b for the melt-reintegrated sample 16ST02*. Biotite and epidote are consumed shortly after crossing the solidus, and plagioclase appears in the assemblage. With the stabilisation of garnet, quartz and hornblende proportions quickly decrease, while the amount of partial melt at closed-system conditions progressively increases. The closed-system granulite-facies assemblage is dominated by clinopyroxene, garnet and melt with minor proportions of plagioclase, orthopyroxene and ilmenite. In an open-system environment, the 7% threshold of melt accumulation is firstly reached around ∼795 °C with the occurrence of garnet. The residual rock produced in an open-system environment is relatively enriched in augite, orthopyroxene, garnet, and plagioclase after experiencing six events of melt drainage up to a temperature of 1000 °C.

4.2.3 Melt compositions generated during prograde metamorphism

Alongside the construction of phase diagrams and the examination of the change in modal proportions of phases involved in metamorphic assemblages, phase equilibrium modelling allows the investigation of the predicted changing compositions of partial melt produced during anatexis. Melt compositions produced by samples 16ST02* and A4 were calculated in steps of 20 °C along an isobaric P–T path at 9.5 kbar and plotted on a modified total alkali-silica (TAS) diagram (Figure 7a; wt.% oxide, anhydrous normalised basis; modified from Middlemost, 1994) and a normative anorthite–albite–orthoclase ternary diagram (Figure 7b). The compositions plotted are those for open-system calculations involving melt loss events of 6% after the accumulation of 7% partial melt. Arrows indicate the temperature at which the respective melt composition was generated.

The initial melt compositions produced by both samples are very similar and plot in the granite field of the TAS diagram (Figure 7a). The initial melt compositions are rich in H_2O (∼15 wt.%) but H_2O contents decrease up temperature and are close to 3 wt.% by 1000 °C (Table 4). On an anhydrous basis these initial melt compositions contain very little FeO and MgO (<0.03 wt.%) with SiO_2 contents around 73 wt.% (Figure 7a). With increasing

temperature, the melts become more anhydrous, and silica-content of both samples decreases to ∼69 wt.% around 900 °C. After this point, the SiO_2 content decreases more strongly with increasing temperature down to 50–53 wt.% at 1050 °C. While the SiO_2 content consistently decreases with increasing temperature, the melt becomes enriched in FeO and MgO, especially at high temperatures where hornblende is lost from the assemblage. The K_2O content of the melt produced by sample A4 increases while biotite or K-feldspar are being successively consumed going up temperature and decreases after they exhausted, akin to melts generated by sample 16ST02*. The Na_2O content of the melts initially decreases but subsequently increases above temperatures of ∼800 °C with no clear correlation to solid phases being consumed or produced.

On the TAS diagram, with increasing temperature, the composition of melt derived from the samples follows a path from the granodiorite field that straddles the diorite–monzonite and gabbroic-diorite–monzodiorite boundary with 16ST02* lying above the boundary and the amphibolite on or just below it (Figure 7a). At the highest temperatures calculated (1050 °C) the melt compositions in 16ST02* are slightly more silicic and richer in alkalis (∼53 wt.% SiO_2, 5.7 wt.% K_2O + Na_2O) than those generated by the amphibolite (∼50 wt.% SiO_2, 4.7 wt.% K_2O + Na_2O).

For the illustration of the data in an An–Ab–Or ternary diagram (Figure 7b), the modelled melt compositions have been recalculated to proportions of solid phases that would form by crystallisation of the melt using Niggli norms (Niggli, 1936). The initial melts generated by both samples lie on the boundary between the trondhjemite and granite fields from which they develop towards more Or-rich assemblages for the first temperature step but diverge strongly in different directions afterwards, reflecting the differences in the stability of K-feldspar in the two. Melts derived from amphibolite A4 trend towards more anorthitic compositions until ∼800 °C from where they progress through the trondhjemite field towards near Or-absent normative compositions. 16ST02*-derived melts trend strongly into the granite field during heating until K-feldspar (or biotite at lower pressures) is completely consumed around 820 °C. After this point, melts become less K_2O-rich with increasing temperature and progress through the granodiorite and tonalite fields and ultimately enter the trondhjemite field at 940 °C. The compositions of the melts derived from both samples at 1050 °C are very similar

even though they developed along different paths in the diagram.

5 DISCUSSION AND CONCLUSIONS

Partial melting is an inherent feature of high grade metamorphic rocks that form in the deep crust. As seen in the exposed roots of orogens worldwide, these deep crustal levels often contain significant proportions of basic rocks, especially those of Archaean age (e.g. Martin, 1994; White et al., 2017), where such rocks are considered a potential source for TTG (Johnson, Brown, Kaus, & VanTongeren, 2014; Moyen, 2011). Examination of their petrological evolution using newly formulated a–x models by Green et al. (2016) allows for constraints to be placed on metamorphic conditions including partial melting. Evidence for anatexis and melt loss in metabasic rocks from the central region of the Lewisian Complex is clearly provided by the preservation of fluid-poor granulite facies assemblages and supporting field observations of *in-situ* leucosomes (Figures 2–3; Johnson et al., 2012).

For this study, mafic rocks dominated by clinopyroxene and plagioclase with varying amounts of garnet, orthopyroxene, hornblende, quartz, and ilmenite were modelled in order to constrain the P–T conditions of formation and the production of melt during Archaean granulite-facies metamorphism. The phase equilibrium modelling undertaken here establishes peak metamorphic conditions for rocks throughout the central region of the Lewisian Complex. Pairs of garnet-absent and garnet-bearing metagabbroic rocks from each sample location have been used in concert to place tight constraints on upper- and lower-pressure limits of metamorphism, which lie in the range 8–10 kbar.

Temperature constraints are somewhat broader, ranging from about 850 °C to over 1050 °C. The lower temperature constraints are provided by the position of the solidus as the samples modelled all showed evidence for partial melting. Upper temperature limits are typically constrained by the upper stability of hornblende in rocks with peak hornblende or by the relative stabilities of garnet and orthopyroxene from each locality's sample pair. However, as with the pressure estimates, there are no apparent significant temperature trends within the central region. Given this, it is likely that the peak temperatures in each locality were similar,

554 at least to within the precision that can be achieved by currently available thermobarometric
555 methods (e.g. Powell & Holland, 2008). In samples where the peak temperatures are better
556 constrained (e.g. 16BA02, Figure 4c), maximum temperatures up to 1000 °C could be inferred
557 (Figure 8).

558 The modelled peak P–T conditions of Badcallian metamorphism are consistent with the
559 findings of Johnson and White (2011). They lie within the range proposed by many earlier
560 studies but do not reach the high-P conditions based on thermobarometry of metasedimen-
561 tary rocks (Cartwright & Barnicoat, 1986, 1987, 1989; Zirkler et al., 2012) or some high-T
562 estimates derived from thermobarometry of mafic and ultramafic granulites from the Scourie
563 area (e.g. O'Hara & Yarwood, 1978). The calculated peak conditions are consistent with the
564 high $\mathrm{d}T/\mathrm{d}P$ (>77.5 °C/kbar) type of metamorphism (Brown & Johnson, 2018), which is
565 interpreted as part of widespread paired metamorphic systems that developed coevally with
566 the amalgamation of dispersed blocks of protocontinental lithosphere in the Neoarchaean.

567 Reaction textures involving the consumption of garnet are consistent with a degree of high-
568 T decompression following peak conditions (Johnson & White, 2011) along a clockwise P–T
569 path with a relatively shallow $\mathrm{d}P/\mathrm{d}T$, with the rocks remaining at mid-crustal depth during
570 cooling. Such a path is also consistent with the growth of garnet subsequent to its breakdown
571 (Figure 8). However, it is unclear whether this later growth of garnet occurred during the
572 later stages of the granulite-facies Badcallian event, or represents a discrete metamorphic
573 overprint during the c. 2.5 Ga Inverian event. Irrespective of the timing, it is consistent
574 with the rocks remaining at depth during both events, as estimated conditions for Inverian
575 amphibolite-facies metamorphism are close to 5 kbar (Cartwright & Barnicoat, 1986; Sills,
576 1982, 1983; Zirkler et al., 2012).

577 Badcallian peak metamorphic conditions show no systematic variation between samples
578 from different localities, even though samples were investigated from throughout the central
579 region, including both the proposed Gruinard and Assynt terranes, but does not discount the
580 possibility of the central region being composed of two distinct terranes (Friend & Kinny,
581 2001; Goodenough et al., 2010; Love, Kinny, & Friend, 2004; Park, 2005). This
582 close similarity in metamorphic conditions is consistent with the central region representing

583 a single coherent block during and subsequent to the Badcallian metamorphic event. Park
584 (2005) suggested that accretion of the Assynt and Gruinard terranes occurred at c. 2.49–2.40
585 Ga, which post-dates the common metamorphic ages of Badcallian metamorphism of c. 2.7–
586 2.8 Ga (e.g. Wheeler et al., 2010; Zirkler et al., 2012). If the Assynt and Gruinard terranes
587 represent truly allochthonous blocks then the close similarity in peak metamorphic conditions
588 throughout the central region is highly fortuitous. Additionally, reaction textures involving
589 the consumption and regrowth of garnet are observed in samples from both proposed terranes,
590 consistent with the post Badcallian evolution being shared among the entire central region.

591 The preservation of granulite-facies mineral assemblages through much of the central
592 region is consistent with the production and loss of significant quantities of partial melt (e.g.
593 Fyfe, 1973; Johnson et al., 2012; Palin et al., 2016b, 2016; Stuck & Diener, 2018; White &
594 Powell, 2002). This conclusion is further supported by widespread field evidence for melting
595 and geochemical evidence showing a consistent depletion in Si, U, Th and some large ion
596 lithophile elements (K, Rb, Cs) compared to amphibolite-facies rocks in the southern region
597 (Johnson et al., 2012; Rollinson, 2012; Rollinson & Windley, 1980).

598 In order to constrain the likely amount and composition of melt produced from the metab-
599 asites, petrological modelling of two approximate protolith compositions was undertaken: one
600 a melt re-integrated granulite from the central region, and the other an amphibolite from the
601 southern region. This procedure assumed that the protoliths were minimally H_2O-saturated
602 at the wet solidus, based on the apparent fluid-saturated conditions of the amphibolite-facies
603 southern region rocks and amphibolite-facies gneiss reported from other Archaean terrains
604 (Garde, 1997; Nehring, Foley, Holtta, & van der Kerkhof, 2009). However, it cannot be
605 conclusively established that all the mafic lithologies of the central region had been fully
606 hydrated during prograde metamorphism. In particular, some larger bodies of layered mafic-
607 ultramafic metagabbro may have potentially escaped complete hydration (Johnson & White,
608 2011), thus limiting their melt fertility (cf. Palin et al., 2016). However, evidence for partial
609 melting in most outcrops is consistent with the protoliths having been hydrous. For fully hy-
610 drated compositions, significant quantities of up to 45 mol.% melt could be produced by each
611 composition under closed-system conditions at the estimated peak P–T conditions (Figure 6b
612 & d). Somewhat lower quantities of about 30 mol.% melt relative to the starting composition

is calculated to have been produced under open-system conditions, which is likely the case. Rocks in the central region commonly preserve leucosomes in various sizes from millimetre to metres, which would allow melt segregation and migration, rather than accumulating in the source rocks.

On a TAS plot, the composition of melt produced in the models ranges from granitic (*sensu lato*) at the wet solidus to roughly dioritic/monzonitic at the interpreted peak P–T conditions of 900–1000 °C (Figure 7a). This is consistent with the composition of felsic to intermediate leucosomes observed in the region (Johnson et al., 2012; Rollinson, 1994). On a normative An–Ab–Or plot, this up-temperature trend in decreasing silica content of the melt for the amphibolite protolith is accompanied by a progression of melt compositions from granite to trondhjemite. By contrast, melt in the melt re-integrated composition remains granitic until about 900 °C where it then changes in composition significantly as it evolves through granodioritic and tonalitic compositions up-grade. This trend shows close match to the compositional spread of the measured felsic sheets in the region (Johnson et al., 2012; Rollinson, 1994) shown on Figure 7b, especially for the amphibolite protolith composition. While much of the more granitic material in these sheets could conceivably have been derived from small batches of earlier-formed, lower-temperature melt from the metabasic units, it could also have been formed from melting of the intermediate- to felsic TTG gneisses in the area (Johnson et al., 2013) as these compositions closely match those predicted by White et al. (2017) for intermediate to felsic TTG gneiss at similar conditions. Considering the high proportion of TTG gneiss compared to the subordinate mafic bodies observed in the field it is likely that the bulk of granitic material was indeed produced from melting of TTG gneiss while partial melts derived from metagabbro may be an important contributor to the more tonalitic sheets. Overall, the field, geochemical and modelling results are consistent with the felsic sheets preserved throughout the central region preserving locally-derived partial melt from the surrounding mafic and most likely also intermediate to felsic gneisses. However, it is noted that the melt compositions discussed here are modelled liquid compositions and do not involve processes such as potential contamination through reaction of the melt with the host rocks or fractional crystallisation.

Modelling of melt production shows that fully hydrated mafic rocks exposed at the current

crustal level appear to have produced and lost a significant volume of melt. Considering a typical geothermal gradient of 30 °C per kilometer (e.g. Brown, 2007) and that the current level of exposure of the central region is around 30 km (∼10 kbar), initial melting of these rocks would have occurred at ∼20 km depth (Figure 6) with subsequently higher proportions of melt being generated at greater depths. Melts that were generated by anatexis of mafic units at greater than 20 km depth likely contributed to a larger proportion of melt derived from felsic to intermediate TTG gneiss (Johnson et al., 2012), and which together formed the source for intrusions at higher crustal levels.

High-temperature metamorphism, melting, and melt extraction are processes critical to understanding crustal evolution and the long-term stabilization of cratonic nuclei (Bickle, 1986). Evidence for these processes are well preserved in the central region of the Archaean Lewisian Gneiss Complex, where temperatures exceeding 900 °C at pressures close to 9 kbar were achieved during the c. 2.7 Ga Badcallian event. Most rock types are expected to melt at such conditions, even if fluid undersaturated (cf. Droop & Brodie, 2012; Johnson, White, & Powell, 2008; Palin et al., 2016). For fully hydrated protoliths, large proportions of melt must be produced and lost to preserve the high-temperature assemblages (White & Powell, 2002). The well-preserved migmatitic mafic gneisses exposed in the central region of the Lewisian Complex thus offer an opportunity to directly investigate and constrain the geological processes that controlled formation and differentiation of the crust during the Archaean. The tectonic environments and geodynamic processes responsible for the stabilization of Earth's first continental nuclei have long been – and remain – a topic of heated debate (e.g. Bédard, 2006; Brown & Johnson, 2018; Foley, Buhre, & Jacob, 2003; Hamilton, 2003; Hawkesworth et al., 2010; Johnson et al., 2017; Palin et al., 2016b; Roberts, Van Kranendonk, Parman, & Clift, 2015).

6 ACKNOWLEDGEMENTS

The research carried out for this study was part of YF's Master Thesis at the Institute of Geoscience, Johannes Gutenberg University, Mainz, which provided the funding for fieldwork and laboratory analyses. TJ acknowledges support from Open Fund GPMR210704 from

the State Key Lab for Geological Processes and Mineral Resources, China University of Geosciences, Wuhan. We thank O. Bartoli, G. Clarke and S. Harley for their perceptive reviews, and M. Brown for his editorial handling.

References

Barnicoat, A. C. (1983). Metamorphism of the Scourian Complex, NW Scotland. *Journal of Metamorphic Geology*, *1*, 163–182.

Beach, A. (1976). The interrelations of fluid transport, deformation, geochemistry and heat flow in early proterozoic shear zones in the lewisian complex. *Philosophical Transactions of the Royal Society of London*, *280*(1298), 569–604.

Bédard, J. H. (2006). A catalytic delamination-driven model for coupled genesis of archaean crust and sub-continental lithospheric mantle. *Geochimica et Cosmochimica Acta*, *70*, 1188–1214.

Bickle, M. J. (1986). Implications of melting for stabilisation of the lithosphere and heat loss in the Archaean. *Earth and Planetary Science Letters*, *80*, 314–324.

Brown, M. (2007). Metamorphic conditions in orogenic belts: a record of secular change. *International Geology Review*, *49*, 193–134.

Brown, M., & Johnson, T. E. (2018). Secular change in metamorphism and the onset of global plate tectonics. *American Mineralogist*, *103*, 181–196.

Cartwright, I., & Barnicoat, A. C. (1986). The generation of quartz-normative melts and corundum-bearing restites by crustal anatexis: petrogenetic modelling based on an example from the Lewisian of North-West Scotland. *Journal of Metamorphic Geology*, *3*, 79–99.

Cartwright, I., & Barnicoat, A. C. (1987). Petrology of Scourian supracrustal rocks and orthogneisses from Stoer, NW Scotland: implications for the geological evolution of the Lewisian complex. In Park, R. G. & Tarney, J. (Ed.), *The evolution the Lewisian and comparable Precambrian high grade terrains* (Vol. 27, pp. 93–107). Geological Society of London, Special Publication.

Cartwright, I., & Barnicoat, A. C. (1989). Evolution of the Scourian complex. In Daly, J.

S., Cliff, R. A. & Yardley, B. W. D. (Ed.), *Evolution of Metamorphic Belts* (Vol. 43, pp. 297–301). Geological Society of London, Special Publication.

Cohen, A. S., O'Nions, R. K., & O'Hara, M. J. (1991). Chronology and mechanism of depletion in Lewisian granulites. *Contributions to Mineralogy and Petrology*, *106*, 142–153.

Corfu, F., Heaman, L. M., & Rogers, G. (1994). Polymetamorphic evolution of the Lewisian complex, NW Scotland, as recorded by U-Pb isotopic compositions of zircon, titanite and rutile. *Contributions to Mineralogy and Petrology*, *117*, 215–228.

Dale, J., Powell, R., White, R. W., Elmer, F. L., & Holland, T. J. B. (2005). A thermodynamic model for Ca–Na clinoamphiboles in Na_2O–CaO–FeO–MgO–Al_2O_3–SiO_2–H_2O–O for petrological calulations. *Journal of Metamorphic Geology*, *23*, 771–791.

Davies, J. H. F. L., & Heaman, L. M. (2014). New u–pb baddeleyite and zircon ages for the scourie dyke swarm: A long-lived large igneous province with implications for the paleaproterozoic evolution of nw scotland. *Precambrian Research*, *249*, 180–198.

Diener, J. F. A., & Powell, R. (2012). Revised activity–composition relations for clinopyroxene and amphibole. *Journal of Metamorphic Geology*, *30*, 131–142.

Diener, J. F. A., White, R. W., & Hudson, T. J. M. (2014). Melt production, redistribution and accumulation in mid-crustal source rocks, with implications for crustal-scale melt transfer. *Lithos*, *201*, 212–225.

Droop, G. T. R., & Brodie, K. H. (2012). Anatectic melt volumes in the thermal aureole of the Etive Complex, Scotland: the roles of fluid-present and fluid-absent melting. *Journal of Metamorphic Geology*, *30*, 843–864.

Evans, C. R. (1965). Geochronology of the Lewisian Basement near Lochinver, Sutherland. *Nature*, *207*, 54–56.

Foley, S. F., Buhre, S., & Jacob, D. E. (2003). Evolution of the Archaean crust by delamination and shallow subduction. *Nature*, *421*, 249–252.

Friend, C., & Kinny, P. D. (2001). A reappraisal of the Lewisian Gneiss Complex: geochronological evidence for its tectonic assembly from disparate terranes in the Proterozoic. *Contributions to Mineralogy and Petrology*, *142*, 198–218.

Fyfe, W. S. (1973). The granulite facies, partial melting and the Archaean crust. *Philosophical*

Transactions of the Royal Society of London, *A273*, 457–461.

Garde, A. A. (1997). Accretion and evolution of an Archaean high-grade grey gneiss–amphibolite complex: the Fiskefjord area, southern West Greenland. *Geology of Greenland Survey Bulletin*, *177*, 115.

Goodenough, K. M., Park, R. G., Krabbendam, M., Myers, J. S., Wheeler, J., Loughlin, S. C., ... Graham, R. H. (2010). The Laxford Shear Zone: an end-Archean terrane boundary? *Geological Society Special Publication, London*, *335*, 103 - 120.

Green, E. C. R., Holland, T. J. B., & Powell, R. (2007). An order–disorder model for omphacitic pyroxenes in the system jadeite–diopside–hedenbergite–acmite, with applications to eclogitic rocks. *American Mineralogist*, *92*, 1181–1189.

Green, E. C. R., White, R. W., Diener, J. F. A., Powell, R., Holland, T. J. B., & Palin, R. M. (2016). Activity–composition relations for the calculation of partial melting equilibria in metabasic rocks. *Journal of Metamorphic Geology*, *34*, 845–869.

Guevara, V. E., & Caddick, M. J. (2016). Shooting at a moving target: phase equilibria modelling of high-temperature metamorphism. *Journal of Metamorphic Geology*, *34*, 209–235.

Hamilton, W. B. (2003). An alternative Earth. *GSA Today*, *13*, 4–12.

Harley, S. L. (1988). Proterozoic granulites from the Rauer Group, East Antarctica. I. Decompressional pressure-temperature paths deducted from mafic and felsic gneisses. *Journal of Petrology*, *29*, 1059–1095.

Hawkesworth, C. J., Dhuime, B., Pietranik, A. B., Cawood, P. A., Kemp, A. I. S., & Storey, C. D. (2010). The generation and evolution of the continental crust. *Journal of the Geological Society of London*, *167*, 229–248.

Hawthorne, F. C., Oberti, R., Harlow, G. E., Maresch, W. V., Martin, R. F., Schumacher, J. C., & Welch, M. D. (2012). Nomenclature of the amphibole supergroup. *American Mineralogist*, *97*, 2031–2048.

Holland, T. J. B., & Powell, R. (1998). An internally consistent thermodynamic dataset for phases of petrological interest. *Journal of Metamorphic Geology*, *16*, 309–343.

Holland, T. J. B., & Powell, R. (2003). Activity–composition relations for phases in petrological calculations: an asymmetric multicomponent formulation. *Contributions to*

Mineralogy and Petrology, *145*, 492–501.

Holland, T. J. B., & Powell, R. (2011). An improved and extended internally consistent thermodynamic dataset for phases of petrological interest, involving a new equation of state for solids. *Journal of Metamorphic Geology*, *29*, 333–383.

Holness, M. B., Cesare, B., & Sawyer, E. W. (2011). Melted rocks under the microscope: microstructures and their interpretation. *Elements*, *7*, 247–252.

Johnson, T., & White, R. W. (2011). Phase equilibrium constraints on conditions of granulite-facies metamorphism at Scourie, NW Scotland. *Journal of the Geological Society, London*, *168*, 147–158.

Johnson, T. E., & Brown, M. (2004). Quantitative constraints on metamorphism in the variscides of southern brittany – a complementary pseudosection approach. *Journal of Petrology*, *45*, 1237–1259.

Johnson, T. E., Brown, M., Gardiner, N., Kirkland, C., & Smithies, R. (2017). Earth's first stable continents did not form by subduction. *Nature*, *543*, 239–242.

Johnson, T. E., Brown, M., Goodenough, K. M., Clark, C., Kinny, P. D., & White, R. W. (2016). Subduction of sagduction? ambiguity in constraining the origin of ultramafic-mafic bodies in the archean crust of nw scotland. *Precambrian Research*, *283*, 89–105.

Johnson, T. E., Brown, M., Kaus, B. J. P., & VanTongeren, J. A. (2014). Delamination and recycling of archaean crust caused by gravitational instabilities. *Nature Geoscience*, *7*, 47–52.

Johnson, T. E., Fischer, S., & White, R. W. (2013). Field and petrographic evidence for partial melting of TTG gneisses from the central region of the mainland Lewisian complex, NW Scotland. *Journal of the Geological Society, London*, *179*, 319–326.

Johnson, T. E., Fischer, S., White, R. W., Brown, M., & Rollinson, H. R. (2012). Archean Intracrustal Differentiation from Partial Melting of Metagabbro - Field and geochemical Evidence from the Central Region of the Lewisian Complex, NW Scotland. *Journal of Petrology*, *53*(10), 2115–2138.

Johnson, T. E., White, R. W., & Powell, R. (2008). Partial melting of metagreywacke: a calculated mineral equilibria study. *Journal of Metamorphic Geology*, *26*, 837–853.

Johnson, Y. A., Park, R. G., & Winchester, J. A. (1987). Geochemistry, petrogenesis and

tectonic significance of the early Proterozoic Loch Maree Group amphibolites of the Lewisian Complex, NW Scotland. *Geological Society, London, Special Publications*, *33*, 255–269.

Kelsey, D. E., White, R. W., & Powell, R. (2003). Orthopyroxene–sillimanite–quartz assemblages: distribution, petrology, quantitative P–T–X constraints and P–T paths. *Journal of Metamorphic Geology*, *21*, 439–453.

Kinny, P. D., Friend, C. R. L., & Love, G. J. (2005). Proposal for a terrane-based nomenclature for the Lewisian Gneiss Complex of NW Scotland. *Geological Society, London*, *162*, 175–186.

Korhonen, F. J., Brown, M., Clark, C., & Bhattacharya, S. (2013). Osumilite–melt interactions in ultrahigh temperature granulites: phase equilibria modelling and implications for the *P–T–t* evolution of the Eastern Ghats Province, India. *Journal of Metamorphic Geology*, *31*, 881–907.

Love, G. J., Kinny, P. D., & Friend, C. R. L. (2004). Timing of magmatism and metamorphism in the gruinard bay area of the lewisian gneiss complex: comparisons with the assynt terrane and implications for terrane accretion. *Contributions to Mineralogy and Petrology*, *146*, 620–636.

Martin, H. (1994). The Archaean grey gneisses and the genesis of continental crust. In K. C. Condie (Ed.), *Archaean crustal evolution. Developments in Precambrian geology* (pp. 205–258). Elsevier, New York.

Middlemost, E. A. K. (1994). Naming materials in the magma/igneous rock system. *Earth-Science Reviews*, *37*, 215–224.

Moorbath, S., Welke, H., & Gale, N. H. (1969). Significance of lead isotope studies in ancient, high-grade metamorphic basement complexes, as exemplified by Lewisian rocks of Northwest Scotland. *Earth and Planetary Science Letters*, *6*, 245–256.

Moyen, J. F. (2011). The composite Archaean grey gneisses: petrological significance, and evidence for a non-unique setting for Archaean crustal growth. *Lithos*, *123*, 21–36.

Muecke, G. K. (1969). *Petrogenesis of granulite facies rocks from the lewisian of north-west scotland.* (Unpubl. D.-thesis, University of Oxford)

Nehring, F., Foley, S. F., Holtta, P. S., & van der Kerkhof, A. M. (2009). Internal differen-

tiation of the Archean continental crust: fluid-controlled partial melting of granulites and TTG-amphibolite associations in central Finland. *Journal of Petrology*, *50*, 3–35.

Niggli, P. (1936). über molekularnormen zur gesteinsberechnung. *Schweizerische Mineralogische und Petrographische Mitteilungen*, *16*, 295–317.

O'Brien, P., & Rotzler, J. (2003). High-pressure granulites: formation, recovery of peak conditions and implications for tectonics. *Journal of Metamorphic Geology*, *21*, 3–20.

O'Hara, M. J. (1961). Zoned ultrabasic and basic gneiss masses in the early lewisian metamorphic complex at scourie, sutherland. *Journal of Petrology*, *2*, 248–276.

O'Hara, M. J. (1977). Thermal history of excavation of archaean gneisses from the base of the continental crust. *Journal of the Geological Society, London*, *134*, 185–200.

O'Hara, M. J., & Yarwood, G. (1978). High pressure–temperature point on an archaean geotherm, implied magma genesis by crustal anatexis, and consequences for garnet–pyroxene thermometry and barometry. *Philosophical Transactions of the Royal Society of London*, *288*, 441–456.

Palin, R. M., Weller, O. M., Waters, D. J., & Dyck, B. (2016c). Quantifying geological uncertainty in metamorphic phase equilibria modelling; a Monte Carlo assessment and implications for tectonic interpretations. *Geoscience Frontiers*, *7*, 591–607.

Palin, R. M., White, R. W., & Green, E. C. R. (2016b). Partial melting of metabasic rocks and the generation of tonalitic–trondhjemitic–granodioritic (TTG) crust in the Archean: constraints from phase equilibria modelling. *Precambrian Research*, *287*, 73–90.

Palin, R. M., White, R. W., Green, E. C. R., Diener, J. F. A., Powell, R., & Holland, T. J. B. (2016). High-grade metamorphism and partial melting of basic and intermediate rocks. *Journal of Metamorphic Geology*, *34*, 871–892.

Park, R. G. (2005). The Lewisian terrane model: a review. *Scottish Journal of Geology*, *41*, 105–118.

Park, R. G., & Tarney, J. (1987). The Lewisian complex: a typical Precambrian high-grade terrain? *Geological Society, London*, *27*, 13–25.

Park, R. G., Tarney, J., & Connelly, N. (2001). The Loch Maree Group: Paleoproterozoic subduction–accretion complex in the Lewisian of NW Scotland. *Precambrian Research*,

105, 205–226.

Pattison, D. R. M. (2003). Petrogenetic significance of orthopyroxene-free garnet + clinopyroxene + plagioclase ± quartz-bearing metabasites with respect to the amphibolite and granulite facies. *Journal of Metamorphic Geology*, *21*, 21–34.

Peach, B. N., Horne, J., Gunn, W., Clough, C. T., Hinxman, L. W., & Teall, J. J. H. (1907). The Geological Structure of the North West Highlands of Scotland. *Memoirs of the Geological Survey U.K.*.

Powell, R., & Holland, T. J. B. (1988). An internally consistent thermodynamic dataset with uncertainties and correlations: 3. Application, methods, worked examples and a computer program. *Journal of Metamorphic Geology*, *6*, 173–204.

Powell, R., & Holland, T. J. B. (2008). On thermobarometry. *Journal of Metamorphic Geology*, *26*, 155–179.

Roberts, N. M. W., Van Kranendonk, M. J., Parman, S., & Clift, P. D. (2015). Continent formation through time. In N. M. W. Roberts, M. J. Van Kranendonk, S. Parman, S. Shirey, & P. D. Clift (Eds.), *Continent Formation Through Time* (Vol. 389, pp. 1–16). Geological Society of London, Special Publications.

Rollinson, H. (1994). Origin of felsic sheets in the Scourian granulites: new evidence from rare earth elements. *Scottish Journal of Geology*, *30*, 121–129.

Rollinson, H. (2012). Geochemical constraints on the composition of Archaean lower continental crust: Partial melting in the Lewisian granulites. *Earth and Planetary Science Letters*, *351*, 1–12.

Rollinson, H., & Windley, B. F. (1980). Selective elemental depletion during metamorphism of Archaean granulites, Scourie, NW Scotland. *Contributions to Mineralogy and Petrology*, *72*, 257–263.

Rollinson, H. R. (1981). Garnet-pyroxene thermometry and barometry in the scourie granulites, nw scotland. *Lithos*, *14*, 225–238.

Rollinson, H. R., & Tarney, J. (2005). Adakties–the key to understanding LILE depletion in granulites. *Lithos*, *79*, 61–81.

Rosenberg, C. L., & Handy, M. R. (2005). Experimental deformation of partially melted granite revisited: implications for the continental crust. *Journal of Metamorphic Geology*,

23, 19–28.

Rudnick, R. L., & Taylor, S. R. (1987). The composition and petrogenesis of the lower crust: A xenolith study. *Journal of Geophysical Research*, *92*, 13981–14005.

Sawyer, E. W. (1991). Disequilibrium melting and the rate of melt–residuum separation during migmatization of mafic rocks from the grenville front, quebec. *Journal of Petrology*, *32*, 701–738.

Sills, J. D. (1982). The retrogression of ultramafic granulites from the Scourian of NW Scotland. *Mineralogical Magazine*, *46*, 55–61.

Sills, J. D. (1983). Mineralogical changes occurring during the retrogression of Archaean gneisses from the Lewisian complex of NW Scotland. *Lithos*, *16*, 113–124.

Sills, J. D., & Rollinson, H. R. (1987). Metamorphic evolution of the mainland Lewisian complex. *Geological Society, London, Special Publications*, *27*, 81–92.

Stuck, T., & Diener, J. F. A. (2018). Mineral equilibria constraints on open-system melting in metamafic compositions. *Journal of Metamorphic Geology*, *in press*.

Sutton, J., & Watson, J. V. (1951). The pre-Torridonian metamorphic history of the Loch Torridon and Scourie areas in the NW Highlands and its bearing on the chronological classification of the Lewisian. *Journal of the Geological Society, London*, *106*, 241–308.

Weaver, B. L., & Tarney, J. (1981). Lewisian gneiss geochemistry and Archean crustal development models. *Earth and Planetary Science Letters*, *55*, 171–180.

Wheeler, J., Park, R. G., Rollinson, H. R., & Beach, A. (2010). The Lewisian Complex: insights into deep crustal evolution. *Geological Society Special Publication, London*, *335*, 51–79.

White, R. W., Palin, R. M., & Green, E. C. R. (2017). High-grade metamorphism and partial melting in Archean composite grey gneiss complexes. *Journal of Metamorphic Geology*, *35*, 181–195.

White, R. W., & Powell, R. (2002). Melt loss and the preservation of granulite facies mineral assemblages. *Journal of Metamorphic Geology*, *20*, 621–632.

White, R. W., & Powell, R. (2010). Retrograde melt–residue interaction and the formation of near-anhydrous leucosomes in migmatites. *Journal of Metamorphic Geology*, *28*, 579–597.

White, R. W., Powell, R., & Clarke, G. L. (2002). The interpretation of reaction textures in Fe-rich metapelitic granulites of the Musgrave Block, central Australia: constraints from mineral equilibria calculations in the system K_2O–FeO–MgO–Al_2O_3–SiO_2–H_2O–TiO_2–Fe_2O_3. *Journal of Metamorphic Geology*, *20*, 41–55.

White, R. W., Powell, R., & Clarke, G. L. (2003). Prograde metamorphic assemblage evolution during partial melting of metasedimentary rocks at low pressures: migmatites from Mt Stafford, central Australia. *Journal of Petrology*, *44*, 1937–1960.

White, R. W., Powell, R., & Halpin, J. A. (2004). Spatially-focussed melt formation in aluminous metapelites from Broken Hill, Australia. *Journal of Metamorphic Geology*, *22*, 825–845.

White, R. W., Powell, R., & Holland, T. J. B. (2001). Calculation of partial melting equilibria in the system Na_2O–CaO–K_2O–FeO–MgO–Al_2O_3–SiO_2–H_2O (NCKFMASH). *Journal of Metamorphic Geology*, *19*, 139–153.

White, R. W., Powell, R., Holland, T. J. B., Johnson, T. E., & Green, E. C. R. (2014). New mineral activity-composition relations for thermodynamic calculations in metapelitic systems. *Journal of Metamorphic Geology*, *32*, 261–286.

White, R. W., Powell, R., Holland, T. J. B., & Worley, B. A. (2000). The effect of TiO_2 and Fe_2O_3 on metapelitic assemblages at greenschist and amphibolite facies conditions: mineral equilibria calculations in the system K_2O–FeO–MgO–Al_2O_3–SiO_2–H_2O–TiO_2–Fe_2O_3. *Journal of Metamorphic Geology*, *18*, 497–511.

Whitehouse, M. J., & Kemp, A. I. S. (2010). On the difficulty of assigning crustal residence, magmatic protolith and metamorphic ages to Lewisian granulites: constraints from combined in situ U-Pb and Lu-Hf isotopes. *Geological Society, London, Special Publications*, *335*, 81–101.

Yakymchuk, C., & Brown, M. (2015). Consequences of open-system melting in tectonics. *Journal of the Geological Society, London*, *171*, 21–40.

Zandt, G., & Ammon, C. J. (1995). Continental crust composition constrained by measurements of crustal Poisson's ratio. *Nature*, *374*, 152–154.

Zhu, Z. K., O'Nions, R. K., Belshaw, N. S., & Gibb, A. J. (1997). Lewisian crustal history from in situ SIMS mineral chronometry and related metamorphic textures. *Chemical*

Geology, *136*, 205–218.

Zirkler, A., Johnson, T. E., White, R. W., & Zack, T. (2012). Polymetmamorphism in the mainland Lewisian complex, NW Scotland - phase equilibria and geochronological constraints from the Cnoc an t'Sidhean suite. *Journal of Metamorphic Geology*, *30*, 865–885.

7 SUPPORTING INFORMATION

Additional Supporting Information may be found online in the supporting information tab for this article.

Supinfo.pdf

Table S1 List of the studied samples with their respective sample locations, rock types, pseudosection figure numbers and bulk rock compositions.

Figures S1–S7 Pseudosections calculated for each sample pair from each location.

Tables and table captions

Table 1: Locality and metamorphic assemblage information for the sixteen samples discussed in this study. Phase abbreviations are after Holland and Powell (1998), alongside 'Fe–Ti ox' for iron–titanium oxides.

Sample	Locality	Observed assemblage
16AC01	Achiltibuie	g, cpx, opx, hb, pl ± Fe–Ti ox
16AC04	Achiltibuie	cpx, opx, hb, pl
16TA07	Tarbet	g, cpx, pl, hb, Fe–Ti ox
16TA08	Tarbet	g, cpx, pl, hb, Fe–Ti ox
16DR03	Drumbeg	g, cpx, pl, Fe–Ti ox ± hb
16DR07	Drumbeg	g, cpx, pl, Fe–Ti ox ± mt
16BS01	Ben Strome	cpx, opx, hb, pl, Fe–Ti ox
16BS05	Ben Strome	g, cpx, pl, Fe–Ti ox ± hb
16SC03	Scourie	cpx, opx, pl, q, Fe–Ti ox
16SC07	Scourie	g, cpx, opx, pl, Fe–Ti ox ± hb
16BA02	Badcall Bay	cpx, opx, pl, Fe–Ti ox ± hb
16BA04	Badcall Bay	g, cpx, opx, pl, Fe–Ti ox ± hb
16ST02	Strathan	g, cpx, opx, pl ± hb ± Fe–Ti ox
16ST03	Strathan	g, cpx, pl, opx, Fe–Ti ox
16AS02	Loch Assynt	cpx, opx, pl, q, Fe–Ti ox ± mt
16AS04	Loch Assynt	g, opx, pl, q, Fe–Ti ox ± hb

Table 2: Bulk-rock compositions used for phase diagram construction (mol.% oxide). FeO^{tot} is total iron expressed as FeO. O is oxygen, which combines with FeO via the equation $2FeO + O = Fe_2O_3$; hence, bulk O is identically equal to bulk Fe_2O_3, while true bulk FeO is given by $FeO^{tot} - 2 \times O$.

Sample	Fig.	H_2O	SiO_2	Al_2O_3	CaO	MgO	FeO^{tot}	K_2O	Na_2O	TiO_2	O	XFe^{3+}
16SC03	**4a**	1.92	55.15	9.67	11.53	7.99	8.15	0.38	3.22	0.61	1.39	0.34
16SC07	**4b**	0.31	45.67	8.70	13.32	15.04	13.40	0.20	0.95	0.80	1.60	0.24
16BA02	**4c**	2.46	50.15	7.82	11.14	14.18	10.29	0.23	2.00	0.47	1.27	0.25
16BA04	**4d**	0.92	49.99	9.03	12.22	7.67	12.98	0.16	2.86	1.49	2.68	0.41
16ST02	**4e**	0.66	50.97	9.06	12.88	13.25	9.25	0.06	2.25	0.51	1.11	0.24
16ST03	**4f**	0.14	50.23	9.13	13.38	12.57	10.87	0.19	1.64	0.71	1.15	0.21
A4	**6c–d**	5.65	50.61	8.46	10.74	10.05	10.38	0.19	2.15	0.91	0.82	0.16

Table 3: Calculated bulk-rock compositions of samples 16BA02, 16BA04, and 16ST02 following melt reintegration (mol.% oxides). The column labelled *Start* gives the starting point of melt reintegration in kbar and °C, respectively. $Melt_{tot}$ and *Steps* give the total amount of melt reintegrated (in mol.%) and the number of reintegration-steps carried out, respectively. Values in square brackets show the difference from the original composition that was used to constrain the conditions of peak metamorphism. The reported bulk composition for undepleted, subsolidus Gairloch amphibolite A4 Johnson et al. (1987) is shown for reference.

Sample	Start	$Melt_{tot}$ / Steps	H_2O	SiO_2	Al_2O_3	CaO	MgO	FeO	K_2O	Na_2O	TiO_2	O
16BA02	8.8 / 920	39 / 6	5.38	53.28	7.94	9.38	11.29	8.42	0.92	2.03	0.37	1.00
			[2.92	3.13	0.12	–1.76	–2.89	–1.87	0.69	0.02	–0.10	–0.27]
16BA04	8.8 / 930	27 / 5	4.52	52.30	8.80	10.31	6.32	10.82	0.63	2.92	1.21	2.17
			[3.60	2.31	–0.23	–1.91	–1.35	–2.16	0.46	0.06	–0.28	–0.51]
16ST02	9.5 / 970	37.5 / 6	4.79	54.23	8.90	10.29	10.03	7.41	0.75	2.39	0.38	0.82
			[4.14	3.26	–0.16	–2.59	–3.21	–1.85	0.69	0.14	–0.14	–0.29]
A4	-	-	5.65	50.61	8.46	10.74	10.05	10.38	0.19	2.15	0.91	0.82

Table 4: Calculated compositions of partial melt generated during prograde metamorphism of melt-reintegrated, granulite-facies sample 16ST02 (cf. Table 3), Strathan, and undepleted, amphibolite-facies sample A4, Gairloch (Johnson et al., 1987). Calculations were performed along an isobaric prograde path at 9.5 kbar under open-system conditions, assuming a 6% melt loss event after the accumulation of 7% of partial melt. Compositions are given as wt% oxide.

Sample	T	H_2O	SiO_2	Al_2O_3	CaO	MgO	FeO	K_2O	Na_2O
16ST02*	625	15.26	61.96	13.48	1.00	0.00	0.02	3.23	5.05
	640	14.24	62.59	13.64	1.16	0.01	0.02	3.67	4.68
	700	10.55	64.77	14.26	1.96	0.01	0.06	5.24	3.14
	760	7.86	66.49	14.63	2.33	0.06	0.29	5.70	2.65
	820	5.46	67.26	14.97	2.76	0.22	1.16	6.10	2.08
	880	4.26	67.16	14.96	3.03	0.56	2.53	5.05	2.44
	940	4.61	65.68	15.05	3.19	1.18	4.23	1.38	4.69
	1000	3.17	57.64	15.10	2.92	3.53	11.13	0.78	5.72
	1050	1.44	52.24	13.50	2.82	6.31	18.05	0.38	5.26
A4	630	15.11	62.09	13.49	1.07	0.01	0.03	3.17	5.03
	640	14.49	62.48	13.60	1.18	0.01	0.03	3.36	4.85
	700	12.32	64.19	13.97	1.79	0.02	0.12	2.91	4.68
	760	10.14	65.66	14.28	2.31	0.08	0.47	2.60	4.46
	820	8.15	66.37	14.51	2.69	0.26	1.45	2.07	4.50
	880	6.37	66.03	14.59	2.85	0.71	3.33	1.16	4.96
	940	5.13	63.49	15.01	3.10	1.56	5.89	0.28	5.54
	1000	3.07	55.60	14.42	3.00	4.02	14.05	0.15	5.69
	1050	1.13	49.86	12.65	3.24	6.02	22.54	0.08	4.47

Figures and figure captions

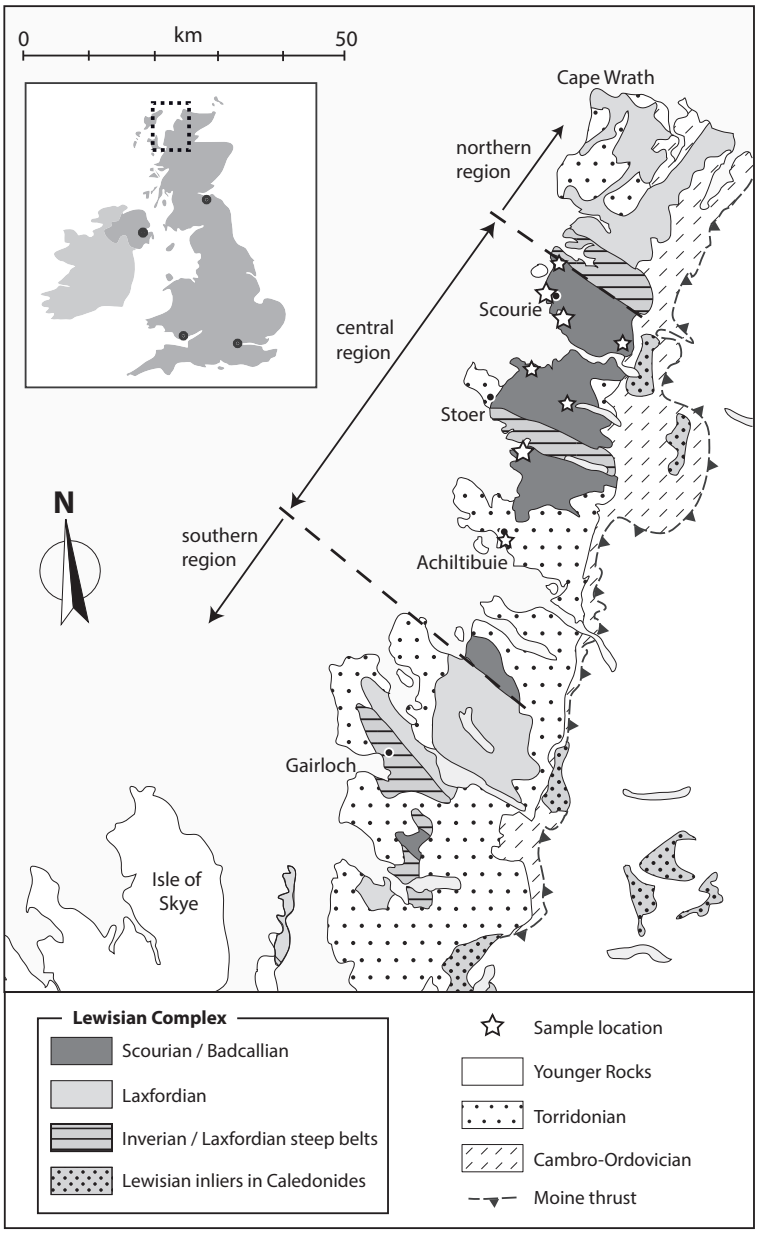

Fig. 1: Map of the mainland Lewisian complex also showing the younger surrounding geology. The central region comprises rocks of granulite facies metamorphic conditions while the northern and southern regions are amphibolite facies. Large stars indicate the sample locations of the representative samples emphasised in this study. Locality names from north to south: Tarbet (TA), Scourie (SC), Badcall Bay (BA), Ben Strome (BS), Drumbeg (DR), Loch Assynt (AS), Strathan (ST), Achiltibuie (AC). Modified after Johnson et al. (2013), and contains British Geological Survey materials ©NERC (2016).

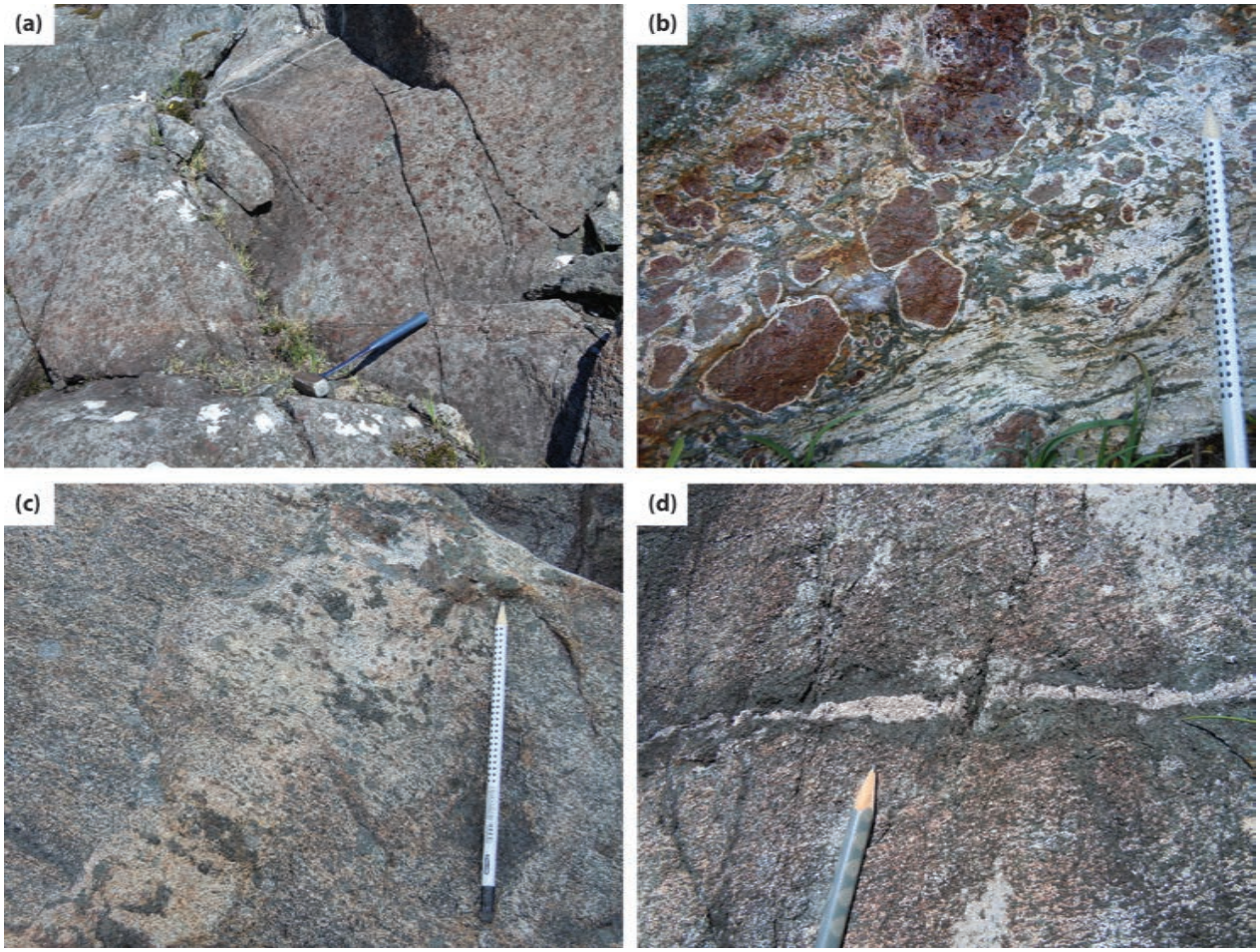

Fig. 2: Outcrop-scale features of Lewisian metagabbroic rocks. **(a)** Garnetiferous metagabbro samples 16TA07 and 16TA08, Tarbet. **(b)** Orthopyroxene- and plagioclase-bearing coronae around large garnet porphyroblasts in sample 16DR03, Drumbeg. Note the ultramafic layer immediately above (top left of photograph) and intermediate leucosome with elongated pyroxenite wisps below (bottom right of photograph). **(c)** *in-situ* derived pyroxene-rich leucosome in garnetiferous metagabbro from Scourie. **(d)** Ultramafic selvedge around injected felsic leucosome within metagabbro sample 16BA02, Badcall Bay.

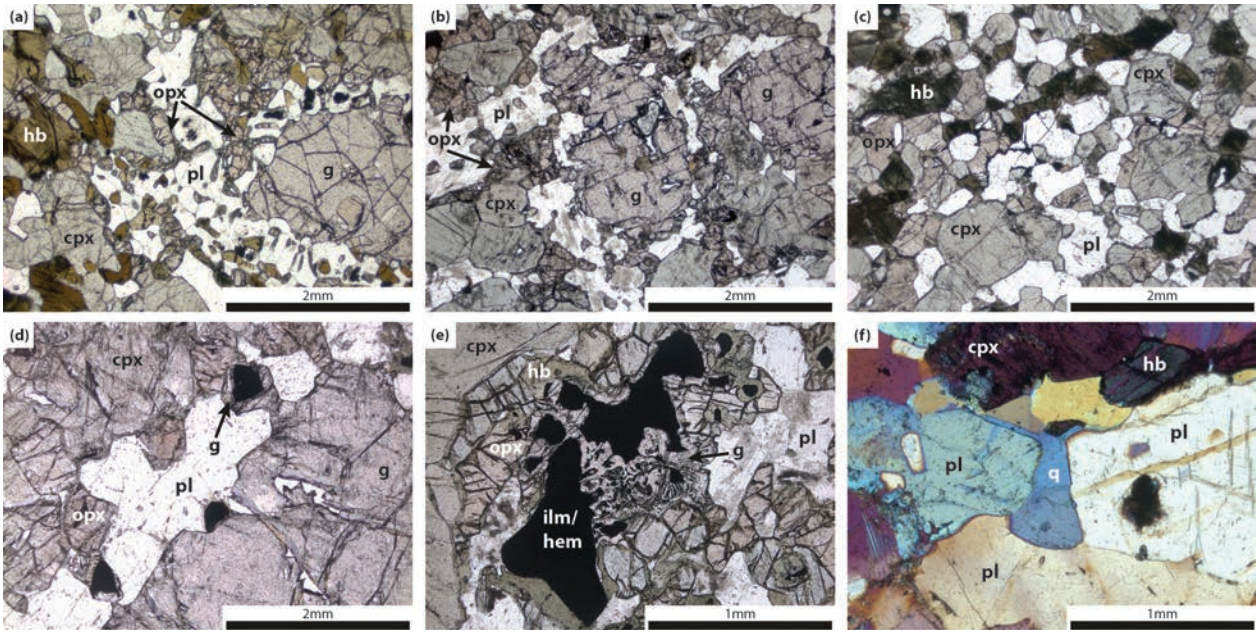

Fig. 3: Thin section-scale petrographic features of Lewisian metagabbroic rocks. **(a)** Representative peak assemblage in sample 16AC01, Achilitibuie, comprised of garnet, orthopyroxene, clinopyroxene, plagioclase and amphibole, showing 120° triple-junctions between plagioclase and pyroxene, and orthopyroxene–plagioclase symplectite development around garnet. **(b)** Representative peak assemblage in sample 16ST03, Strathan. Textures and mineralogy is very similar to (a) but without hornblende. **(c)** Typical peak assemblage in sample 16BA04, Badcall Bay, comprised of eu- to subhedral grains of clinopyroxene, orthopyroxene and plagioclase together with subhedral hornblende in a garnet-absent assemblage. Note the high proportion of fine grained oxides in hornblende. **(d)** Garnet mantling opaque phase in plagioclase-rich corona in sample 16ST02. **(e)** Large grains of Fe–Ti oxide (ilmenohematite) being mantled by garnet and hornblende in sample 16SC07, Scourie. Note symplectic intergrowths of garnet and opaques. **(f)** Petrographic evidence for partial melting in sample 16SC03, Scourie, given by a thin quartz film interpreted to have crystallised in the space between plagioclase and mafic phases, forming small dihedral angles on its grain boundaries.

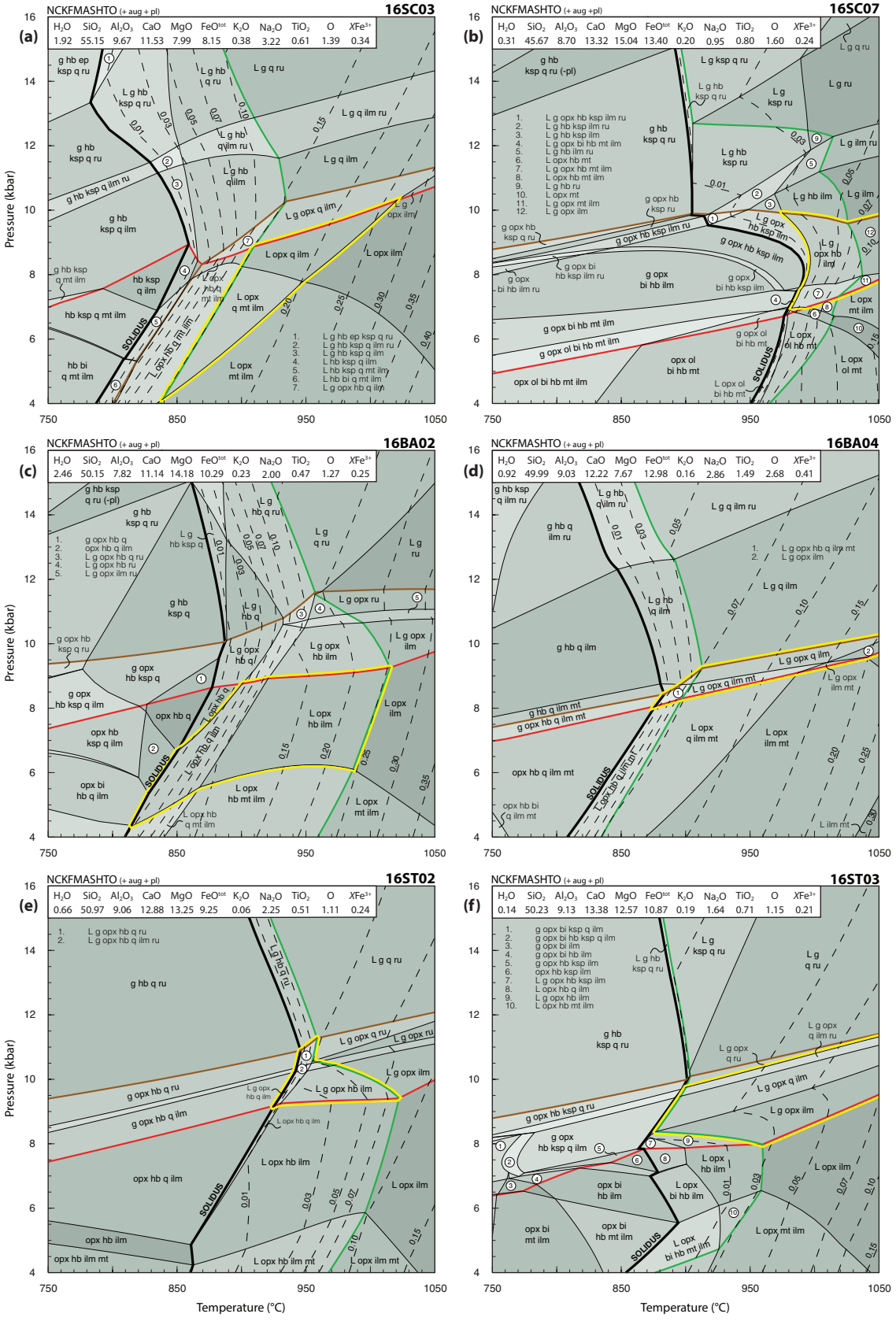

Fig. 4: caption overleaf

Fig. 4: (continued) Calculated P–T pseudosections for the six representative samples discussed in the main text. Compositions are given in mol.%. Assemblage fields interpreted to represent granulite-facies peak assemblages in each individual sample are outlined in yellow boxes. **(a)** Sample 16SC03, Scourie. Peak assemblage: cpx–opx–pl–q–ilm **(b)** Sample 16SC07, Scourie. Peak assemblage: g–cpx–opx–pl–ilm ± hb **(c)** Sample 16BA02, Badcall Bay. Peak assemblage: cpx–opx–pl–ilm ± hb **(d)** Sample 16BA04, Badcall Bay. Peak assemblage: g–cpx–opx–pl–ilm ± q, hb **(e)** Sample 16ST02, Strathan. Peak assemblage: g–cpx–opx–hb–pl ± ilm **(f)** Sample 16ST03, Strathan. Peak assemblage: g–cpx–opx–pl–ilm. The solidi and melt mode contours are indicated by a thick black line and thin dashed lines, respectively. The limits of garnet-bearing, orthopyroxene-bearing, and hornblende-bearing assemblage fields are coloured by red, brown, and green lines, respectively.

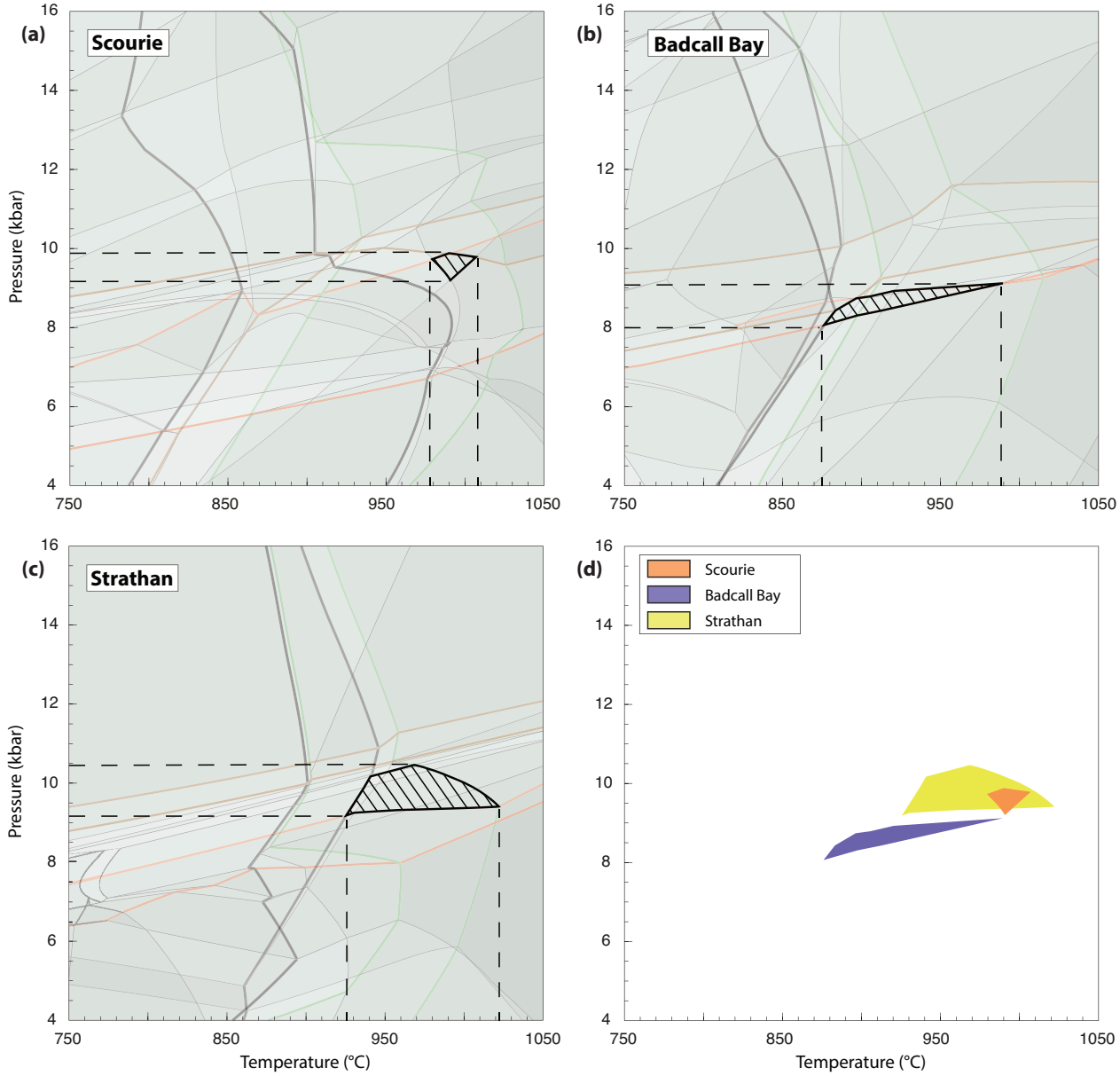

Fig. 5: Overlapping pseudosections of samples emphasized in this study. **(a)–(c)** Combined pseudosections of each two samples from Scourie (16SC02 and 16SC07), Badcall Bay (16BA02 and 16BA04) and Strathan (16ST02 and 16ST03) showing the range of inferred P–T conditions for each locality. **(d)** Compilation of the inferred P–T ranges of the three localities emphasised in this study ((a)–(c)).

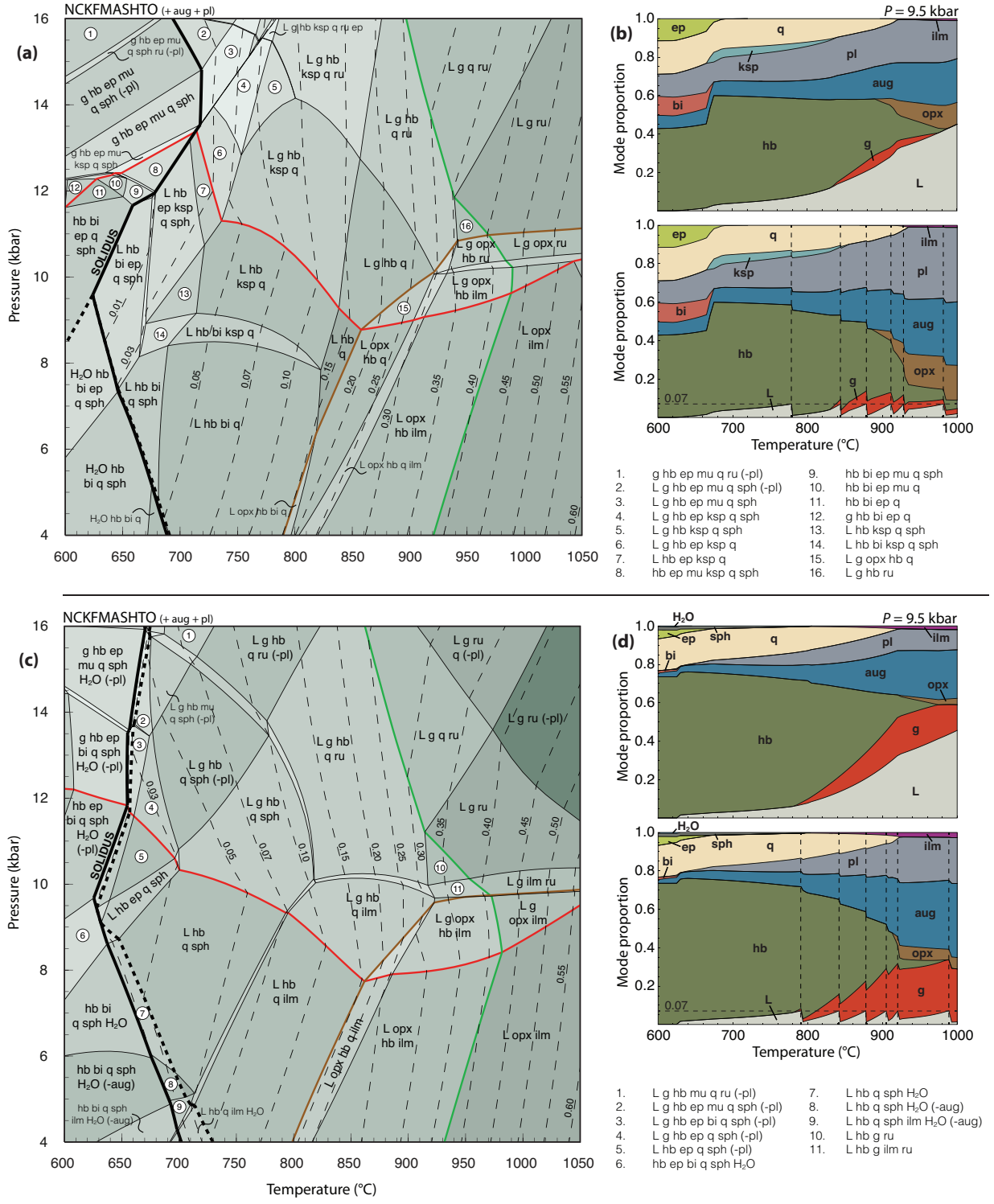

Fig. 6: Calculated P–T pseudosections for bulk-rock compositions not modified by melt loss. **(a)** Bulk composition for sample 16ST02* following melt re-integration. Note the distinctively different assemblage field topologies to those calculated for the residual equivalent (Fig. 4e).

Fig. 6: (continued) **(b)** Modebox diagram showing predicted phase assemblage changes at 9.5 kbar during the prograde evolution of sample 16ST02*, in both a closed-system (upper) and open-system (lower) environment. **(c)** Pseudosection calculated for amphibolite sample A4 from Gairloch, southern region of the Lewisian Complex (Johnson et al., 1987), that did not experience partial melting and/or melt loss during metamorphism. See Table 3 for bulk composition. Note the strong resemblance to the pseudosection in Fig. 6a. **(d)** As for part (b), but for Gairloch amphibolite A4.

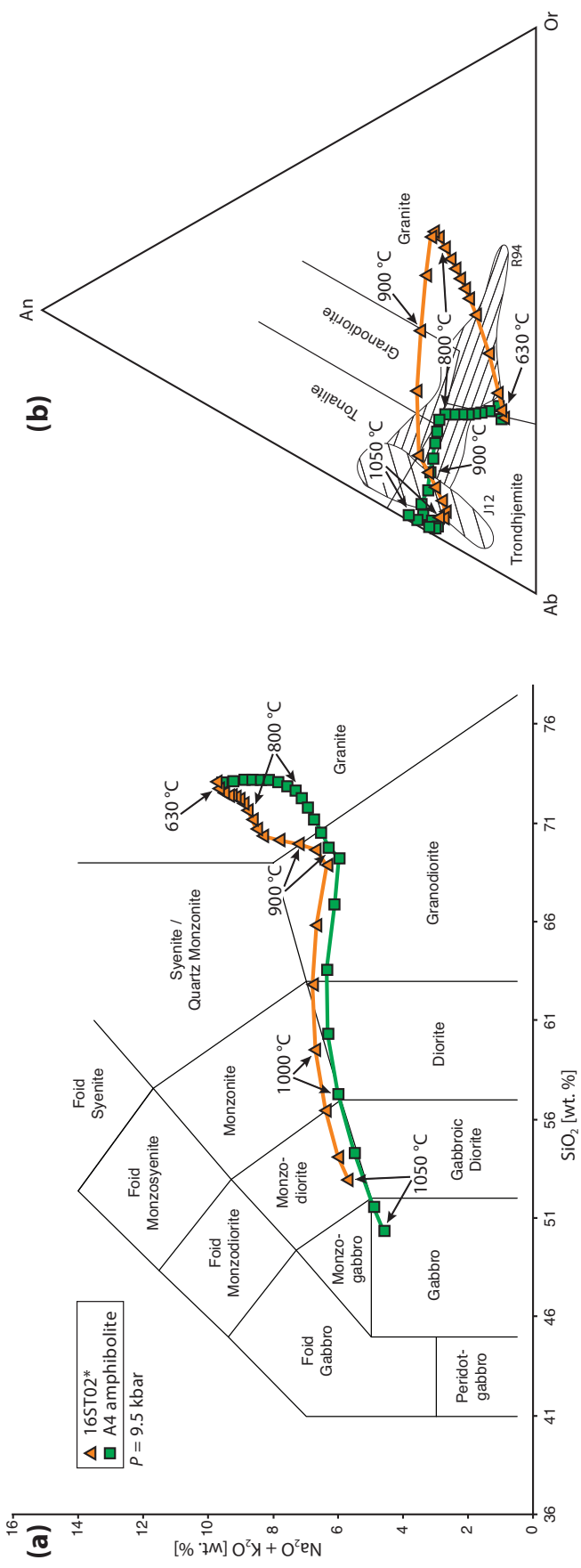

Fig. 7: Calculated melt compositions predicted to form in a melt-reintegrated Lewisian granulite and a Lewisian amphibolite at 9.5 kbar, considering open-system conditions. **(a)** Modified total alkali vs. silica (TAS) diagram showing melts progressing from granitic to intermediate/basic compositions. Field boundaries and labels are after Middlemost (1994), considering the intrusive lithological equivalents to the melts produced. **(b)** Ternary An–Ab–Or diagram comparing Niggli normative proportions (Niggli, 1936) expected to form in crystallised melts discussed in this study to proportions of felsic sheets from the central region Lewisian complex. Modified after Johnson et al. (2012). Data for comparison from: R94 – Rollinson (1994); J12 – Johnson et al. (2012).

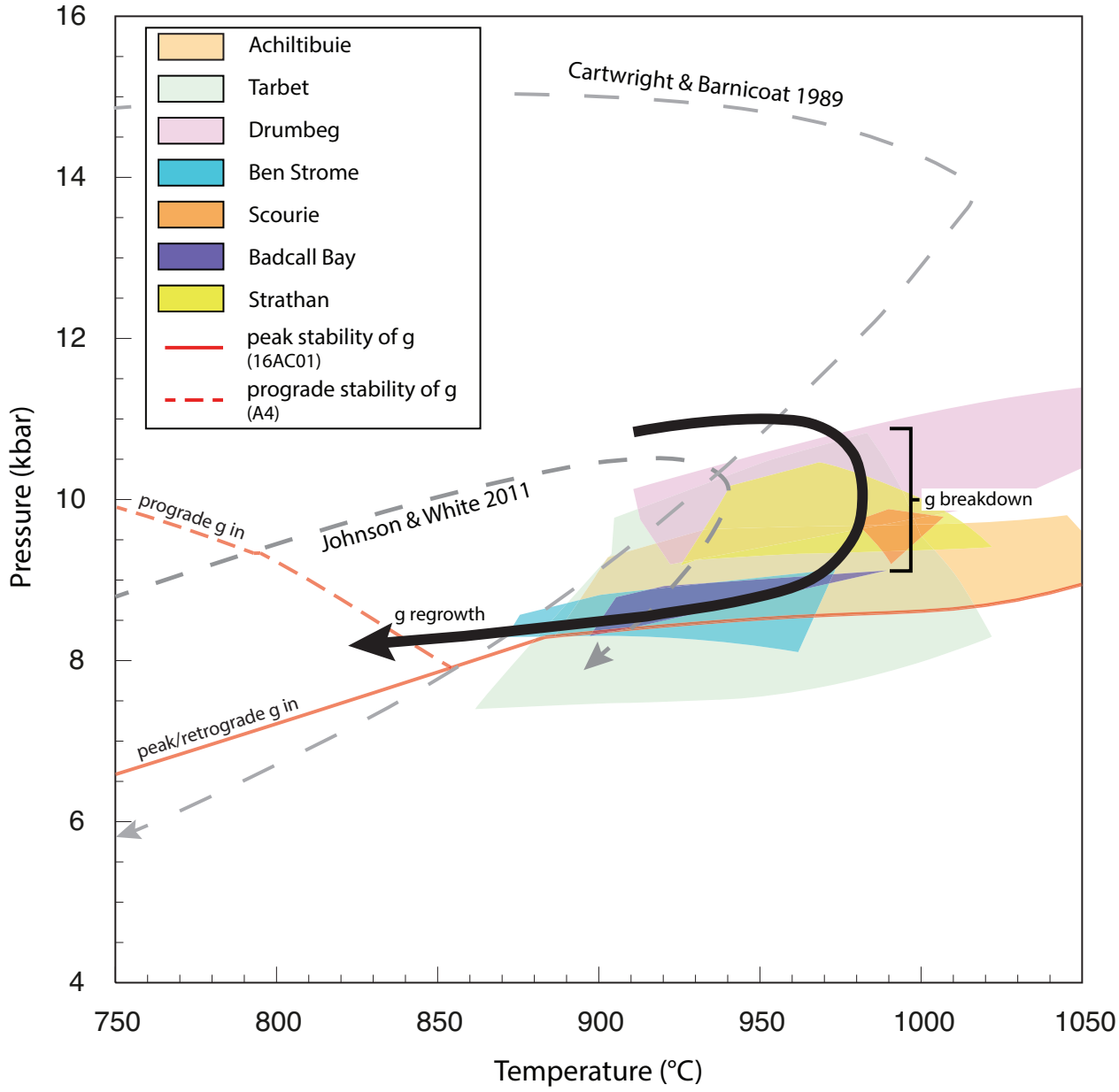

Fig. 8: *P–T* diagram summarising the results of phase equilibrium modelling and showing a proposed *P–T* path based on the findings of this study. The coloured areas illustrate the *P–T* conditions constrained from the sample pairs of each location. Loch Assynt samples are not considered here due to strong retrograde recrystallisation leading to high uncertainties for the interpretation of their peak metamorphic assemblages. Dashed and solid red lines indicate prograde and retrograde/peak garnet stability of samples A4 and 16AC01, respectively. Near isothermal decompression closely after peak conditions is followed by cooling at mid-crustal depths, as interpreted from garnet-microstructures. *P–T* paths of Cartwright and Barnicoat (1989) and Johnson and White (2011) are plotted for comparison.

SUPPLEMENTARY MATERIAL

Table S 1: List of the studied samples with their respective sample locations, rock types, pseudosection figure numbers and bulk rock compositions. Bulk compositions are reduced to the NCKFMASHTO system and recalculated to molar proportions for phase equilibria modelling with THERMOCALC.

Sample	GPS coord.	Rock Type	Fig.#	H_2O	SiO_2	Al_2O_3	CaO	MgO	FeO	K_2O	Na_2O	TiO_2	O	XFe^{3+}	XMg
16AC01	NC 03247 08035	g-bearing metagabbro	S 1	1.01	48.48	7.86	14.37	15.12	10.21	0.19	1.35	0.41	1.01	0.20	0.60
16AC04	NC 03247 08035	g-absent pyroxenite	S 1	2.72	47.36	6.73	11.25	19.41	9.41	0.29	1.40	0.39	1.03	0.22	0.67
16TA07	NC 16893 49589	g-bearing metagabbro	S 2	2.17	51.18	12.24	12.27	8.21	9.55	0.19	2.67	0.79	0.74	0.16	0.46
16TA08	NC 16893 49589	g-bearing metagabbro	S 2	2.18	49.53	11.11	13.92	9.85	9.96	0.28	1.81	0.62	0.74	0.15	0.50
16DR03	NC 11204 32869	g-bearing metagabbro	S 3	4.31	46.44	9.10	13.56	11.58	11.02	0.27	1.62	0.71	1.39	0.25	0.51
16DR07	NC 13330 32491	g-bearing metagabbro	S 3	0.87	49.57	8.32	13.89	7.84	12.24	0.13	2.91	1.09	3.15	0.52	0.39
16BS01	NC 25969 35894	g-absent metagabbro	S 4	2.24	52.05	8.68	11.16	10.33	9.99	0.45	2.83	0.59	1.69	0.34	0.51
16BS05	NC 25759 35900	g-bearing ultramafic	S 4	1.78	45.37	8.30	13.88	12.92	14.59	0.26	0.95	0.72	1.23	0.17	0.47
16SC03	NC 14289 45021	g-absent interm. metagabbro	S 5	1.92	55.15	9.67	11.53	7.99	8.15	0.38	3.22	0.61	1.39	0.34	0.49
16SC07	NC 14197 44180	g-bearing metagabbro	S 5	0.31	45.67	8.70	13.32	15.04	13.40	0.20	0.95	0.80	1.60	0.24	0.53
16BA02	NC 14623 41727	g-absent metagabbro	S 6	2.46	50.15	7.82	11.14	14.18	10.29	0.23	2.00	0.47	1.27	0.25	0.58
16BA04	NC 14624 41840	g-bearing metagabbro	S 6	0.92	49.99	9.03	12.22	7.67	12.98	0.16	2.86	1.49	2.68	0.41	0.37
16ST02	NC 09181 20156	g-bearing metagabbro	S 7	0.66	50.97	9.06	12.88	13.25	9.25	0.06	2.25	0.51	1.11	0.24	0.59
16ST03	NC 09552 20096	g-bearing metagabbro	S 7	0.14	50.23	9.13	13.38	12.57	10.87	0.19	1.64	0.71	1.15	0.21	0.54

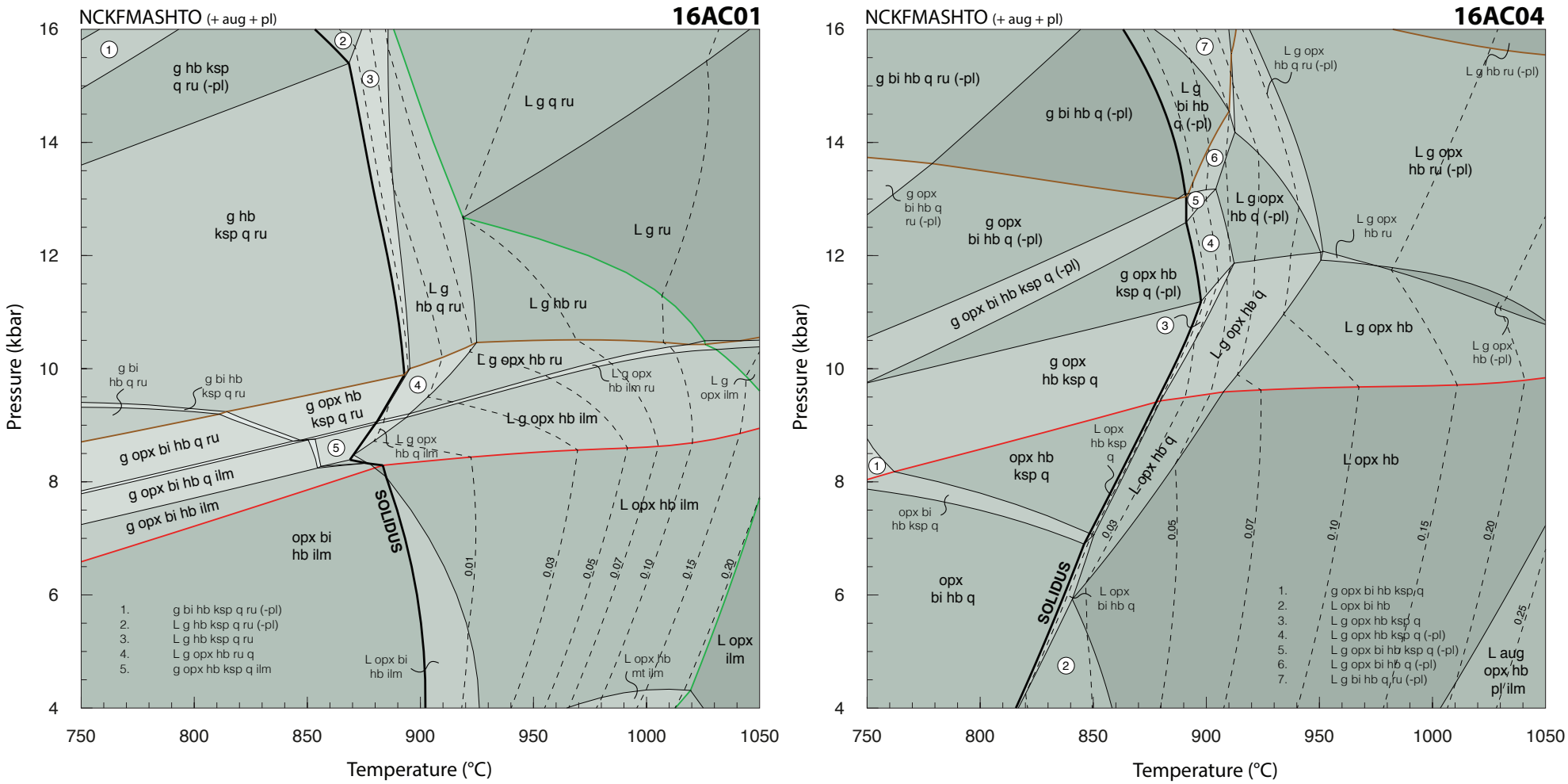

Fig. S 1: Pseudosections calculated for samples from Achiltibuie. (left) 16AC01 (right) 16AC04

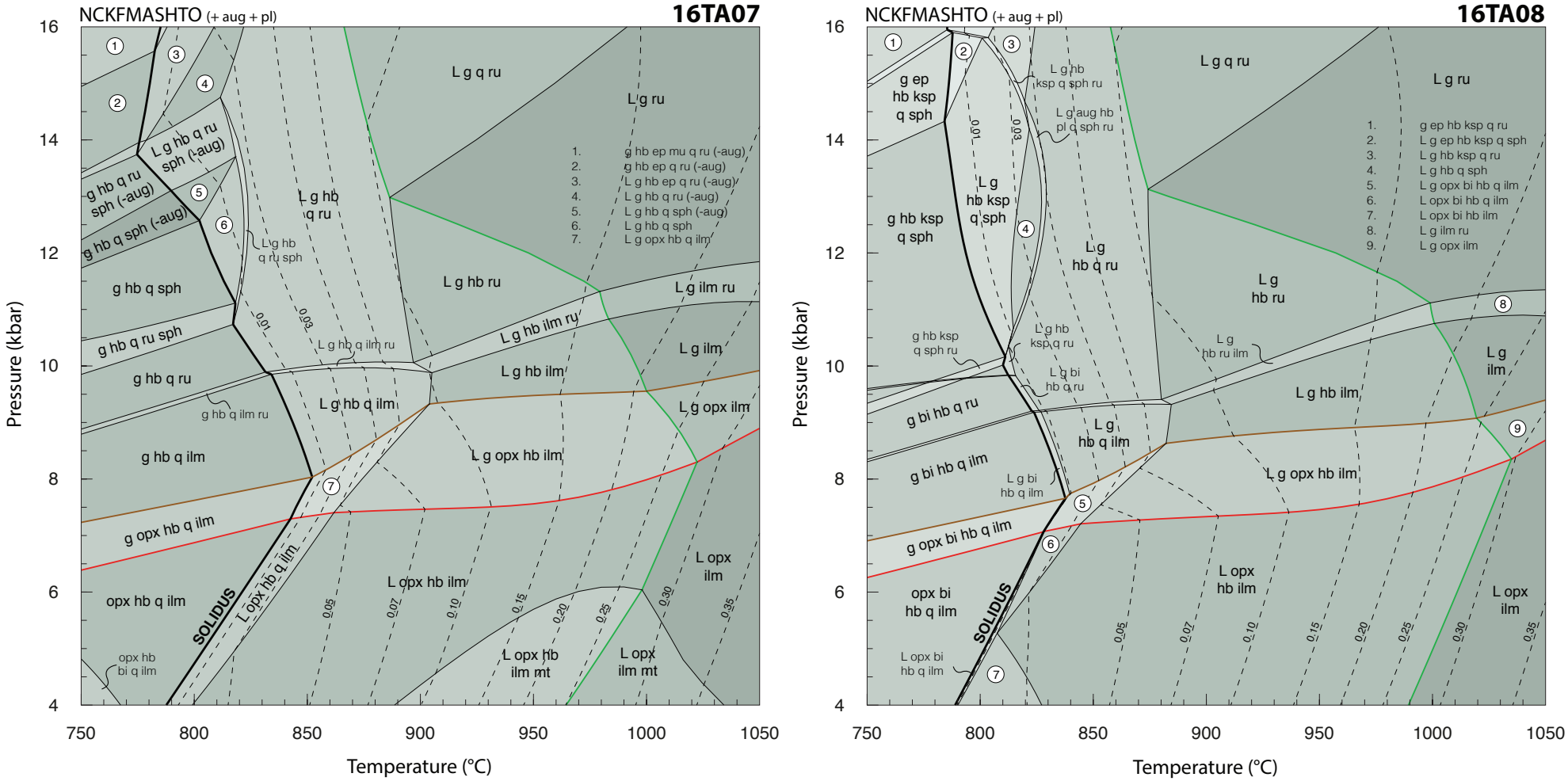

Fig. S 2: Pseudosections calculated for samples from Tarbet. (left) 16TA07 (right) 16TA08

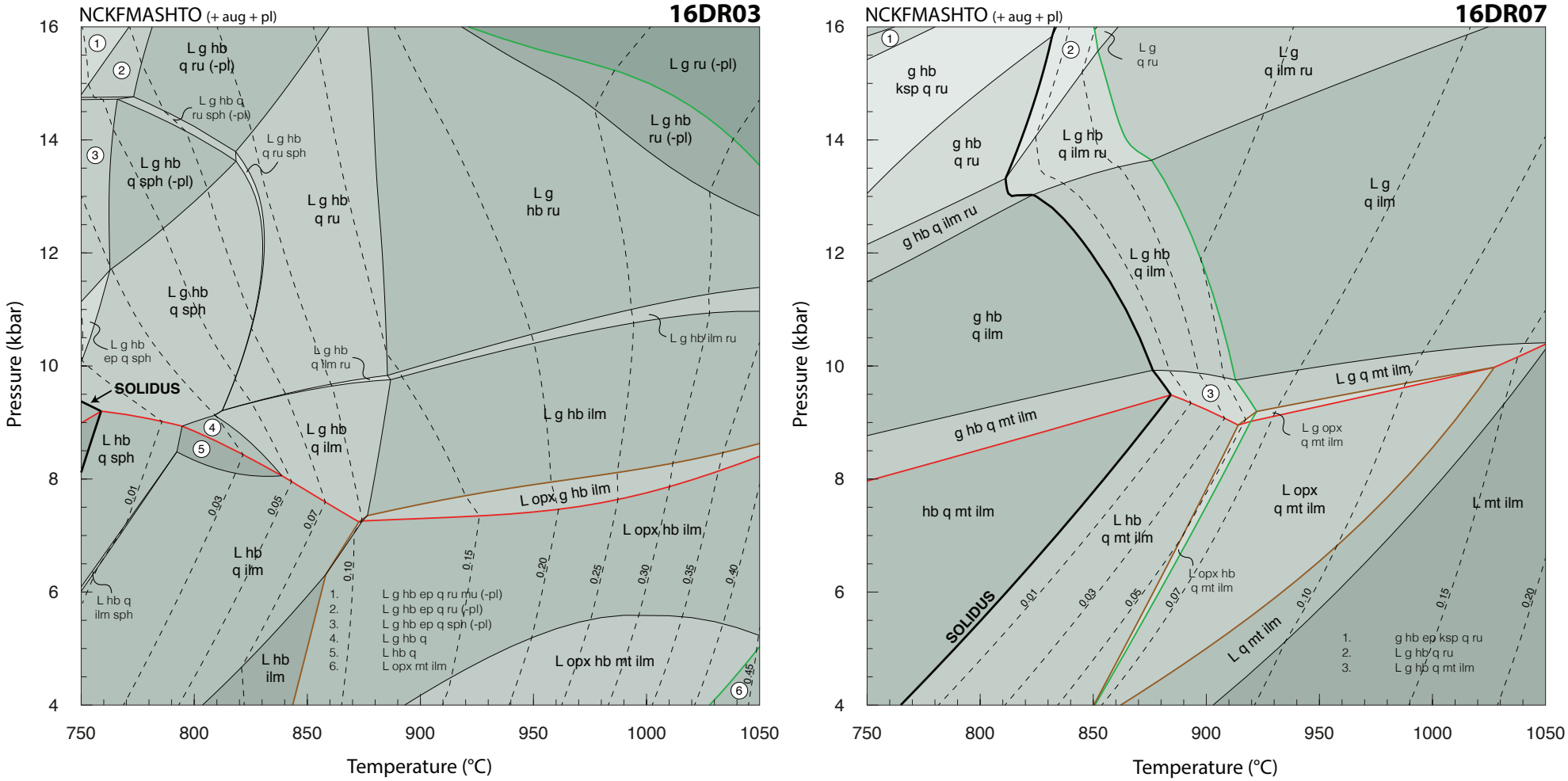

Fig. S 3: Pseudosections calculated for samples from Drumbeg. (left) 16DR03 (right) 16DR07

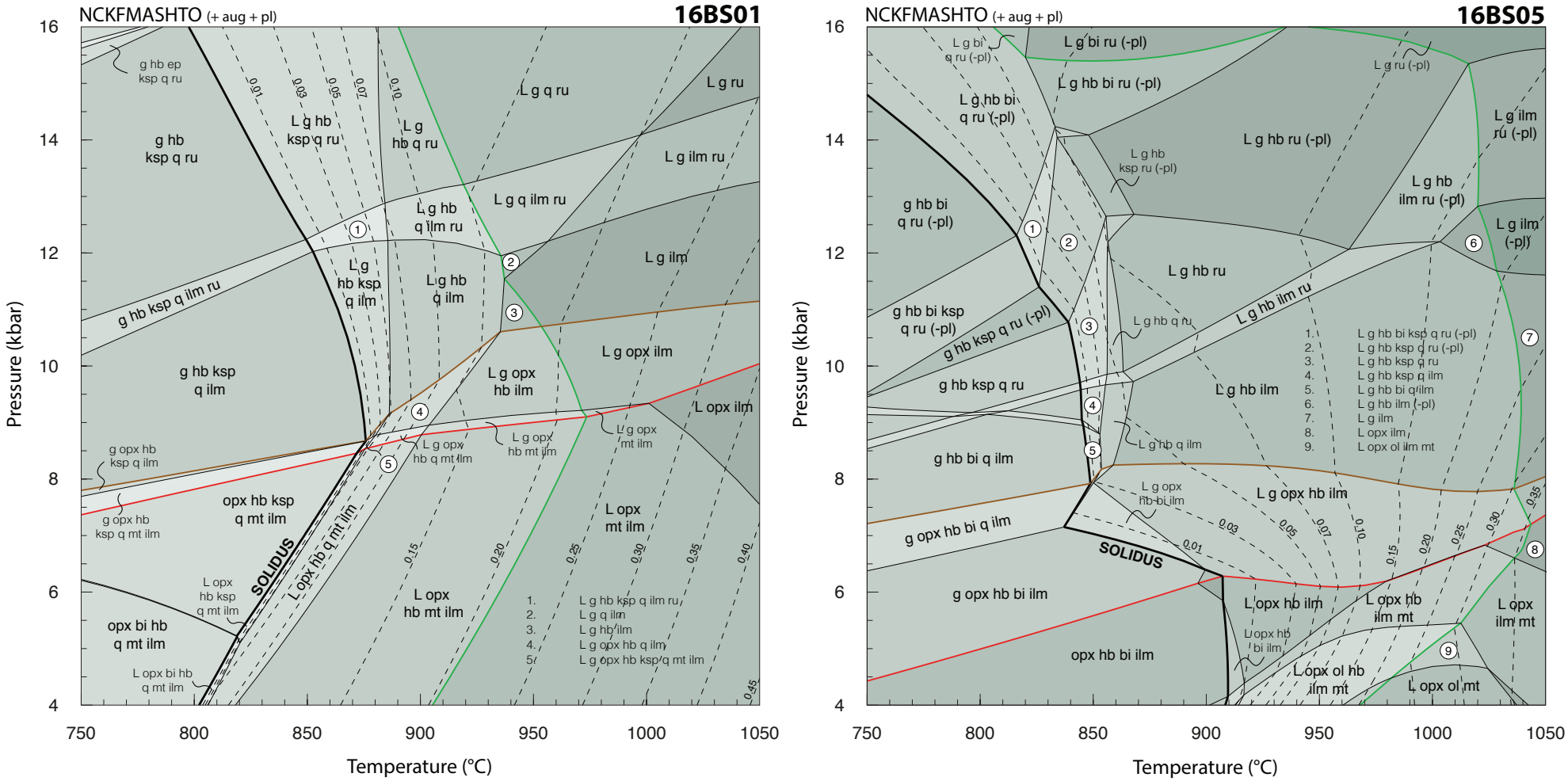

Fig. S 4: Pseudosections calculated for samples from Ben Strome. (left) 16BS01 (right) 16BS05

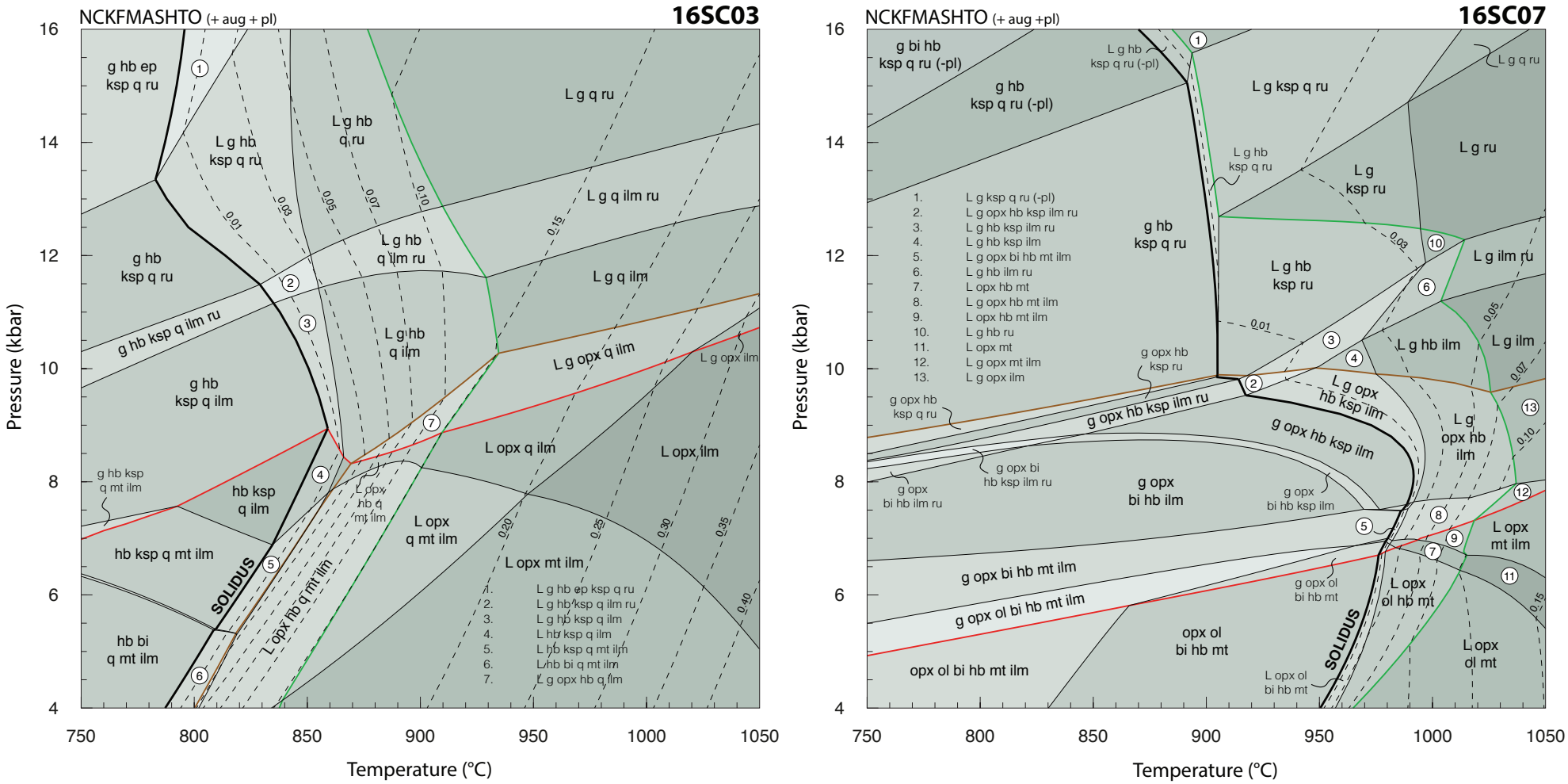

Fig. S 5: Pseudosections calculated for samples from Scourie. (left) 16SC03 (right) 16SC07

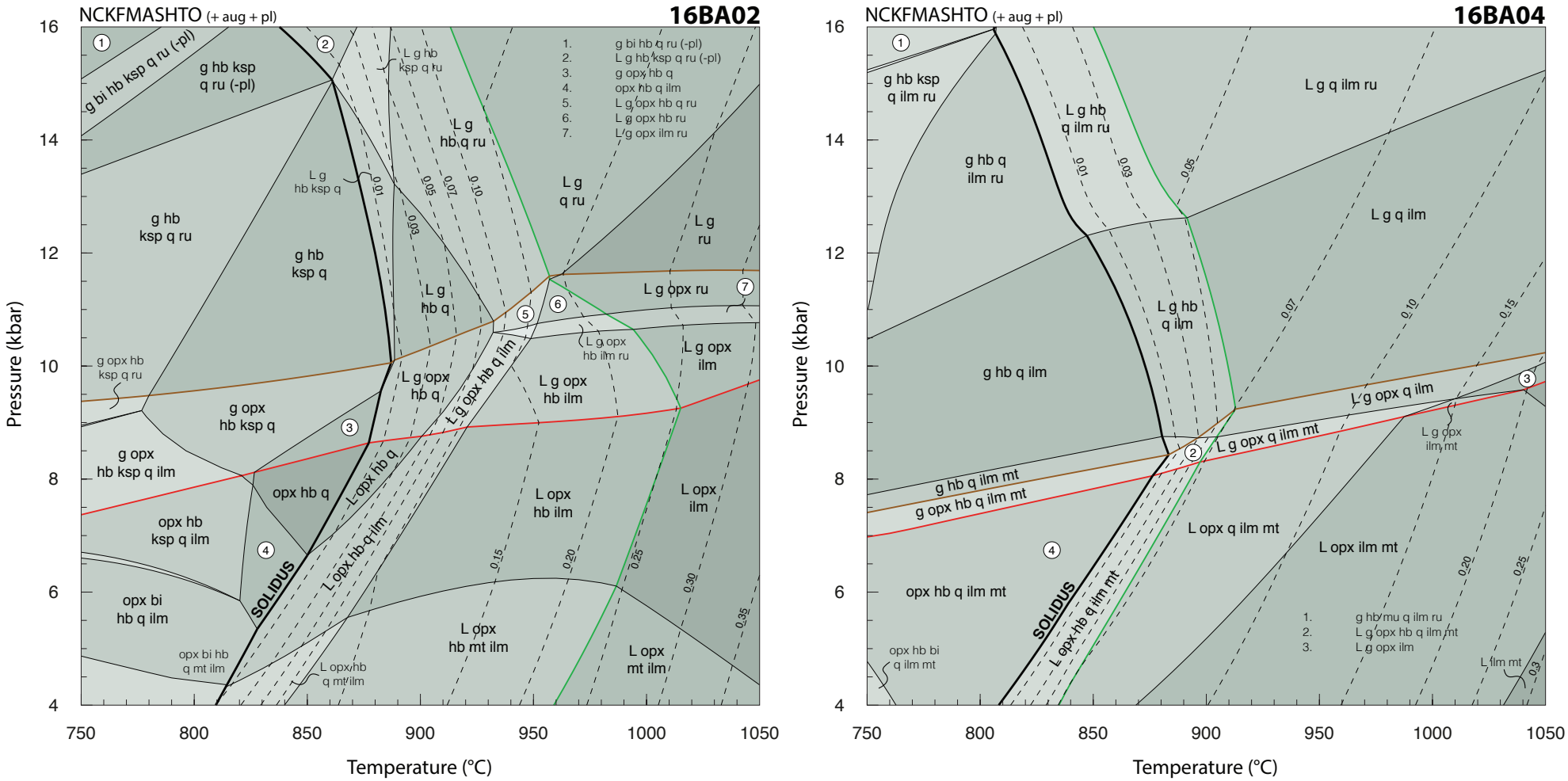

Fig. S 6: Pseudosections calculated for samples from Badcall Bay. (left) 16BA02 (right) 16BA04

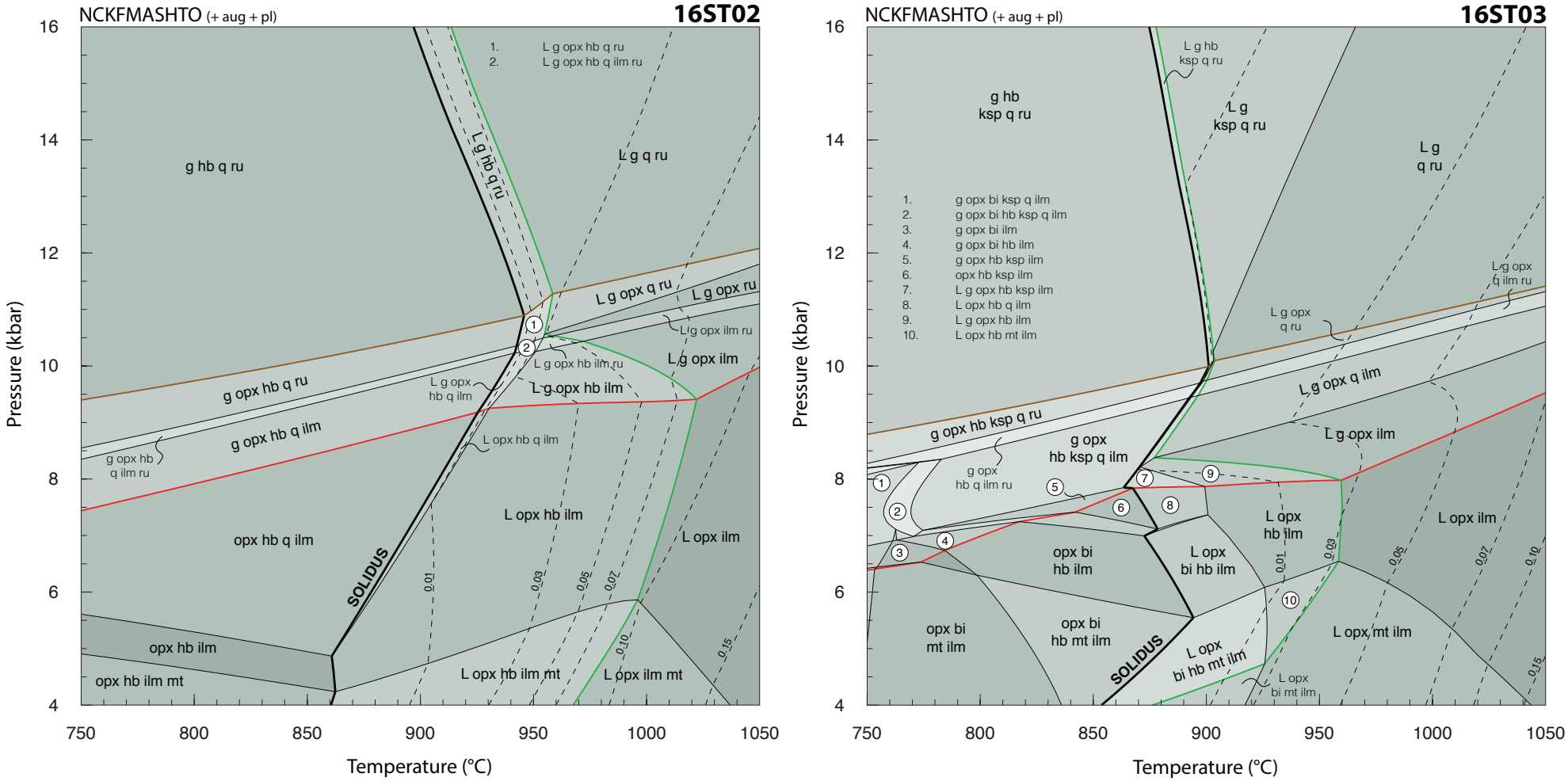

Fig. S 7: Pseudosections calculated for samples from Strathan. (left) 16ST02 (right) 16ST03